Supplementary Information for

In-plane Polarity Boosts Photocatalytic Overall Water Splitting in Two-Dimensional Covalent Organic Frameworks with Polarized Linkages

Yingcai Fan*[, a], Zhihua Zhang[b], Xikui Ma*[, c], Mingwen Zhao*[, b]

[a] *School of Information and Electronic Engineering, Shandong Technology and Business University, Yantai, 264005, China*

[b] *School of Physics, Shandong University, Jinan, 250100, China*

[c] *Center for Optics Research and Engineering of Shandong University, Shandong University, Qingdao, 266237, China*

To whom correspondence should be addressed.

*Email: zmw@sdu.edu.cn (M. Zhao).

42 pages, 1 text, 2 table, 33 figures

Text. Computational details

NAMD calculation. Our nonadiabatic molecular dynamics (NAMD) simulation were carried out by Hefei-NAMD code[1], employing the quantum-classical decoherence-induced surface-hopping (DISH) technique[2-4]. The systems are heated to 300 K by repeated velocity rescaling. Then, a 1 ps microcanonical AIMD trajectory is obtained with a 1 fs atomic time step. The single-Γ-point wave functions of the 1 ps AIMD trajectory were generated with the PBE functional. Using the molecular dynamics trajectory, the NAMD results are based on averaging over 50 different initial configurations with 20000 trajectories. For the simulation of the e-h recombination dynamics on a nanosecond time scale, the 1 ps nonadiabatic Hamiltonians are iterated 1000 times.

Optical absorption calculation. The optical absorption properties were calculated by converting the complex dielectric function to the absorption coefficient α_{abs} according to the following expression[5]:

$$\alpha_{\text{abs}} = \sqrt{2}(\sqrt{\varepsilon_1^2(\omega) + \varepsilon_2^2(\omega)} - \varepsilon_1(\omega))^{\frac{1}{2}}$$

where $\varepsilon_1(\omega)$ and $\varepsilon_2(\omega)$ are the real and imaginary parts, respectively, of the frequency-dependent complex dielectric function $\varepsilon(\omega)$.

Free energy calculation. To compute the free energy change (ΔG) in the HER and OER, we adopted the method developed by Nørskov *et al*[6-10]:

$$\Delta G = \Delta E + \Delta E_{ZPE} - T\Delta S + \Delta G_U + \Delta G_{pH}$$

where ΔE, ΔE_{ZPE} and ΔS are the differences in DFT total energy, zero-point energy and entropy of the two states before and after reaction, respectively. T is the system

temperature (298 K, in our work). ΔG_U represents the contribution of photogenerated electrode potential (U_e/U_h) to ΔG, which is relative to the normal hydrogen electrode (NHE). $\Delta G_{pH} = 0.059 \times pH$ represents the free-energy contribution due to the variations in H concentration. For each system, its E_{zpe} for each adsorbate and free molecules can be calculated by summing vibrational frequencies over all normal modes ν ($E_{zpe} = 1/2\Sigma\hbar\nu$), where only the vibrational modes of the adsorbed intermediates were explicitly computed, while the catalysts were fixed. The entropies of the free molecules were taken from the standard tables in Physical Chemistry[11], while the entropies of adsorbate, derived from their vibrational frequencies, were calculated using the thermodynamics model within the harmonic approximation[12], and the entropies contribution from the catalytic sites was neglected. For those reactions involving the release of protons and electrons, the free energy of one pair of proton and electron ($H^+ + e^-$) was taken as $1/2G_{H2}$. The free energy of O_2(g) was determined by $G_{O2} = 2G_{H2O} - 2G_{H2} - 4.92$ eV since O_2 in triplet ground state is poorly described by DFT calculations[13].

In the aqueous solution, the OER process generally involves four-electron oxidation steps, which can be written as:

$$H_2O+*\rightarrow OH*+H^++e^-$$

$$OH*\rightarrow O*+ H^++e^-$$

$$O*+ H_2O\rightarrow OOH*(O*OH*)+H^++e^-$$

$$OOH*(O*OH*)\rightarrow *+O_2(g)+H^++ e^-$$

Where * denotes the adsorption site, OH*, O* and OOH* denote the adsorbed intermediates.

Meanwhile, the HER process with two-electron pathways, including a fast ptoton/electron transfer step and a fast hydrogen release step, can be written as:

$$*+ H^+ + e^- \rightarrow H^*$$

$$H^* + H^+ + e^- \rightarrow * + H_2(g)$$

Then, the free energy change for OER electrochemical steps can be expressed as:

$$\Delta G_1 = G_{OH^*} + 1/2G_{H_2} - G_{H_2O} - G^* - 0.059 \times \mathrm{pH} - eU$$

$$\Delta G_2 = G_{O^*} + 1/2G_{H_2} - G_{OH^*} - 0.059 \times \mathrm{pH} - eU$$

$$\Delta G_3 = G_{OOH^*(O^*OH^*)} + 1/2G_{H_2} - G_{H_2O} - G_{O^*} - 0.059 \times \mathrm{pH} - eU$$

$$\Delta G_4 = 2G_{H_2O} + G^* - 3/2G_{H_2} - G_{OOH^*(O^*OH^*)} + 4.92 - 0.059 \times \mathrm{pH} - eU$$

The free energy change for HER electrochemical step can be expressed as:

$$\Delta G_{H^*} = G_{H^*} - 1/2G_{H_2} - G^* + 0.059 \times \mathrm{pH} - eU$$

Where 0.059 × pH represents the free energy contribution due to the variations in H concentration, eU represents the effect of a potential bias on all states involving one electron or hole in the electrode by shifting the energy, and U is the electrode potential relative to the normal hydrogen electrode (NHE).

The overpotential (η) can be calculated by the following equations：

$$\eta^{HER} = -|\Delta G_{H*}|/e$$

$$\eta^{OER} = \Delta G_{max}/e - 1.23$$

where ΔG_{H*} and ΔG_{max} are the free energy changes of hydrogen adsorption in the HER process and potential-determining steps (PDS) in the OER process, respectively.

AIMD calculation. The AIMD simulations were carried out under the NVT ensemble (T=300 K). The temperature was controlled by the weak coupling to a Nose-Hoover thermostat. The simulation time for each system was 3 ps with a time step of 1 fs.

Table S1. Values used for the entropy and zero-point energy corrections in determining the free energy of reactants, products, molecules and intermediate species. The ZPE and *TS* values of gaseous molecules were obtained from the standard tables in Physical Chemistry[14].

Species	ZPE (eV)	TS (eV)	ZPE-TS (eV)
H_2	0.29	0.41	-0.12
H_2O	0.60	0.59	0.01
$^*H$	0.18	0.01	0.17
$^*OH$	0.32	0.07	0.25
$^*O$	0.07	0.02	0.05
$^*OOH$	0.42	0.10	0.32

Table S2. Bader charge difference (ΔQ) for Im-TPB, Hy-TPB, Am-TPB, Im-TPP, Hy-TPP and Am-TPP monolayers.

COFs	Δ Q (|e|)						
	Core A	Core B	N (linkages)	CH (linkages)	CO (linkages)	NH (linkages)	CHH (linkages)
Im-TPB	-0.30	-1.31	1.21	-0.68	--	--	
Hy-TPB	-0.19	-0.30	0.69	-0.62	-0.28	0.38	--
Am-TPB	0.03	-1.13	--	--	--	0.79	-0.42
Im-TPP	-0.34	-1.71	1.21	0.69	--	--	--
Hy-TPP	-0.26	-0.33	0.70	-0.63	-0.28	0.36	--
Am-TPP	0.06	-1.87	--	--	--	0.76	-0.42

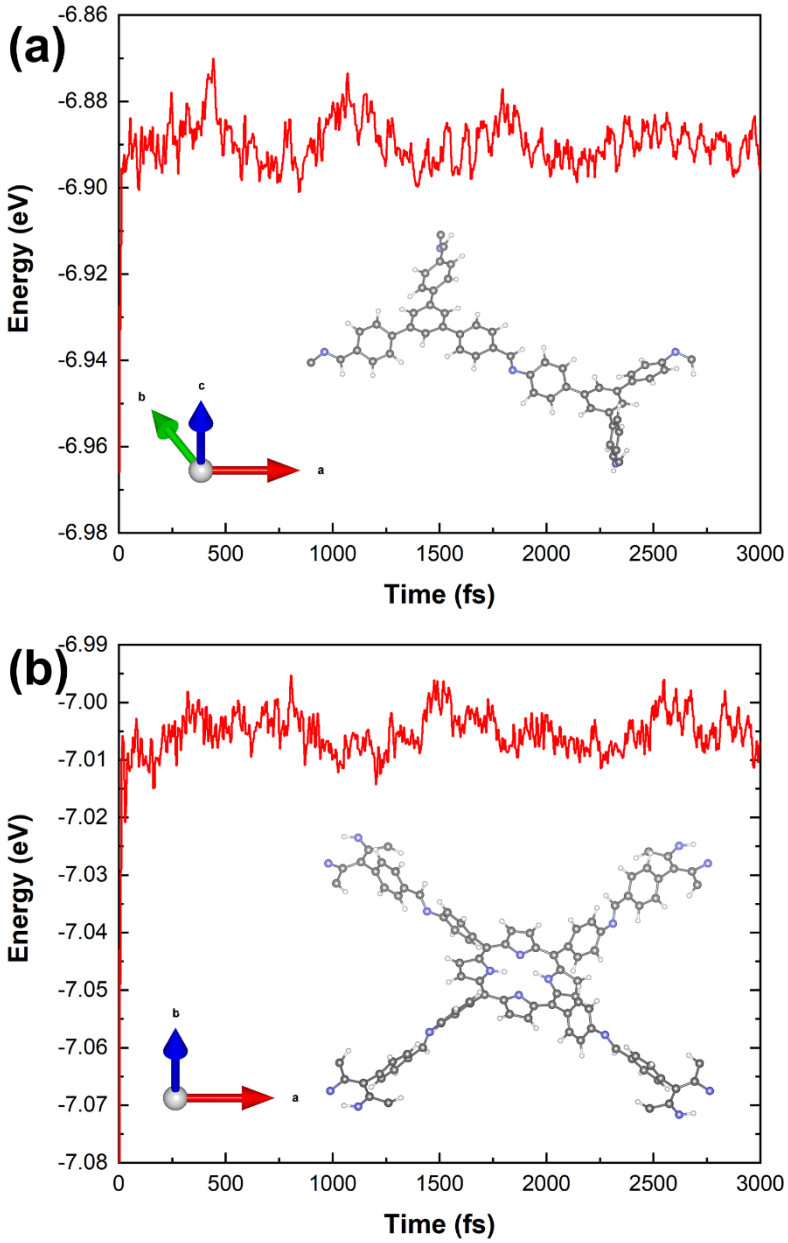

Figure S1. Variations of total energies per atom with the time of AIMD simulations for the (a) Im-TPB and (b) Im-TPP monolayers. The inserts are the structures of the two COFs after AIMD simulations at 300 K for 3000 fs.

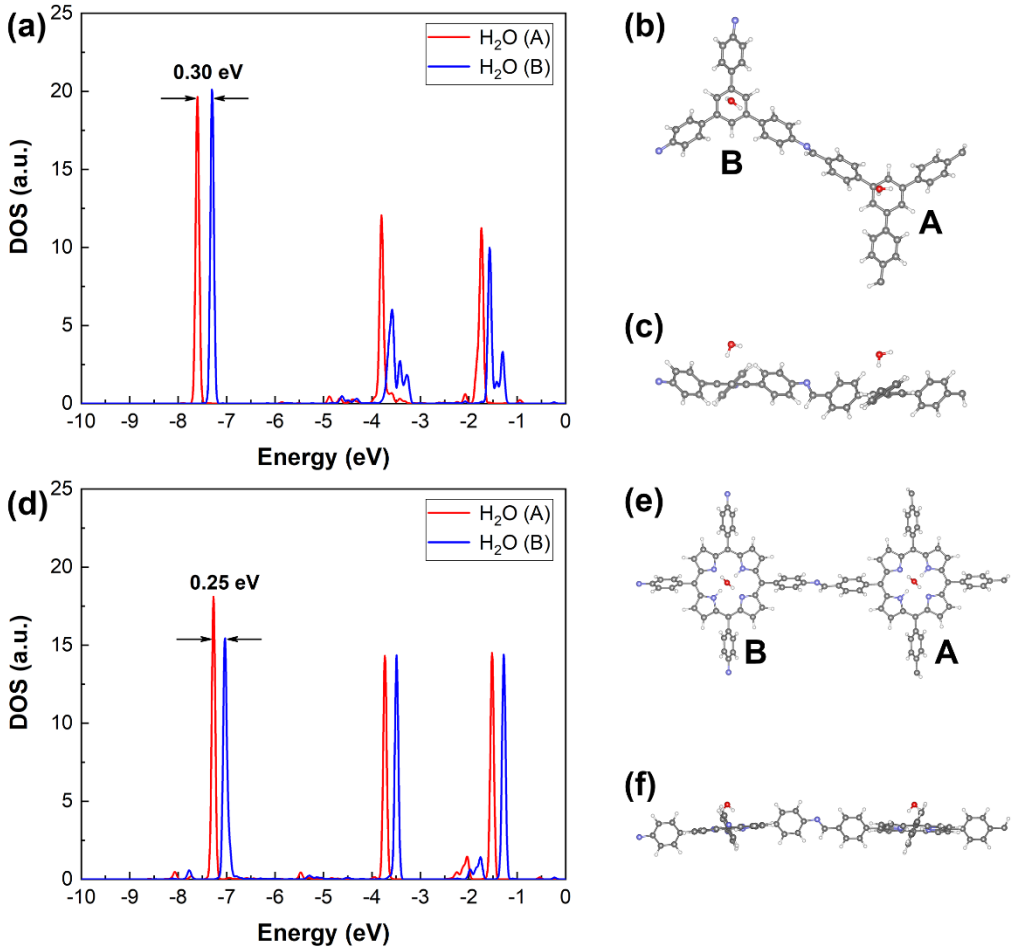

Figure S2. The projected DOS of H_2O molecules adsorbed on the Core A and Core B of (a) Im-TPB and (d) Im-TPP monolayers, respectively. The (b) top and (c) side views of H_2O molecules adsorbed on the Core A and Core B of Im-TPB, respectively. The (e) top and (f) side views of H_2O molecules adsorbed on the Core A and Core B of Im-TPP, respectively.

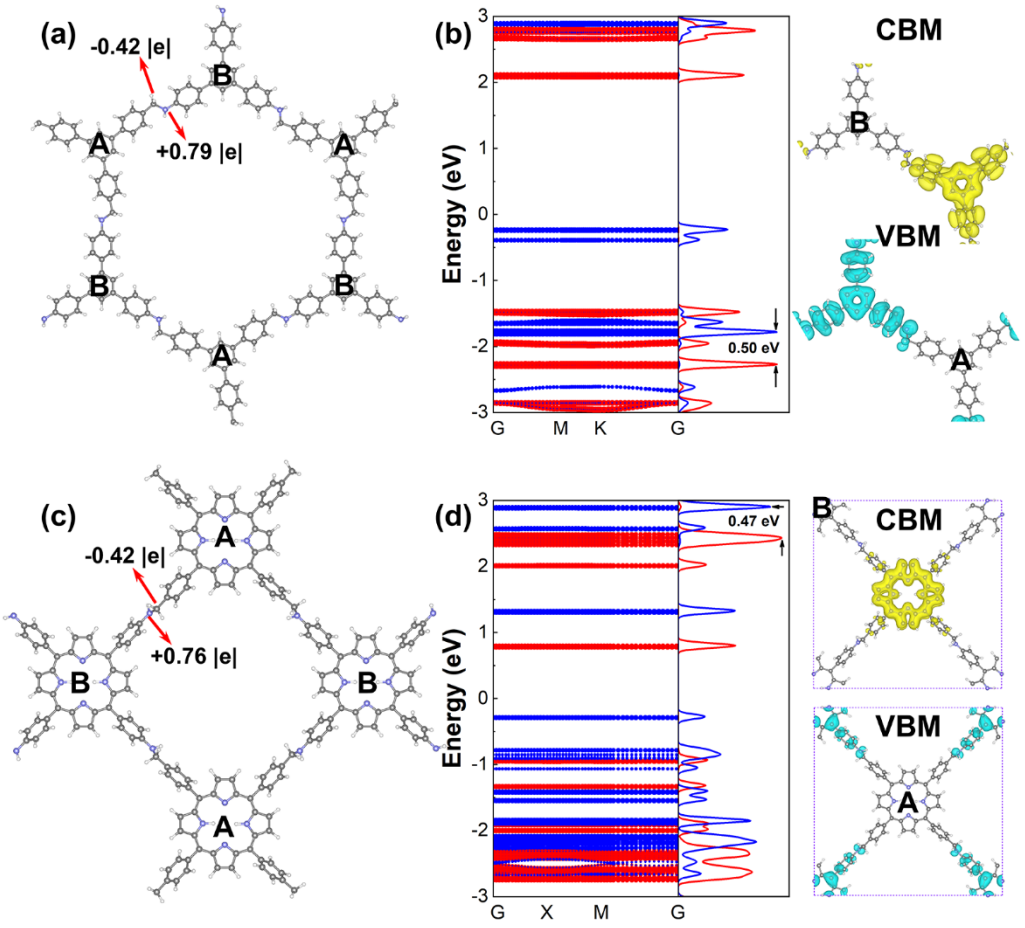

Figure S3. Optimized structures of (a) Am-TPB and (c) Am-TPP COFs monolayers, respectively, where C, N and H atoms are represented by gray, blue and white balls, respectively. Band structures of (b) Am-TPB and (d) Am-TPP projected onto the Core A (red) and Core B (blue) based on the PBE functional, respectively. The right column presents the decomposed charge densities of CBM and VBM. The yellow and bluish areas stand for the CBM and VBM with a contour surface of 0.004 |e|/Å^3.

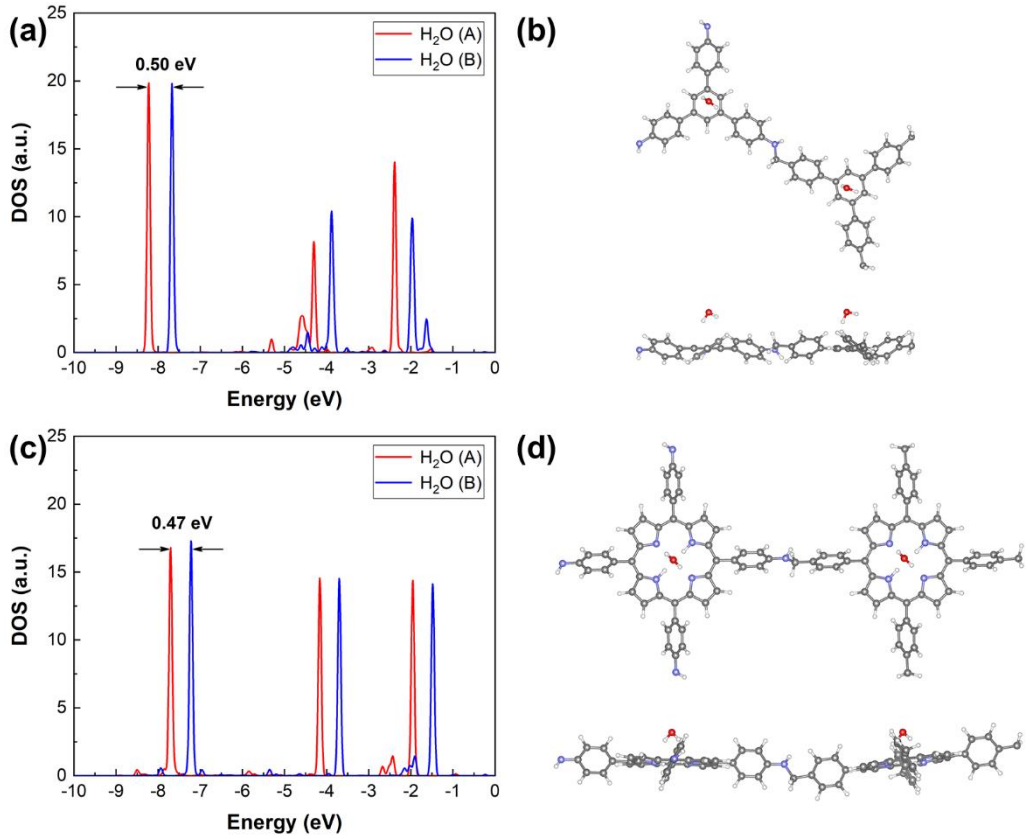

Figure S4. The projected DOS of H_2O molecules adsorbed on the Core A and Core B of (a) Am-TPB and (c) Am-TPP monolayers, respectively. The top and side views of H_2O molecules adsorbed on the Core A and Core B of (b) Am-TPB and (d) Am-TPP monolayers, respectively.

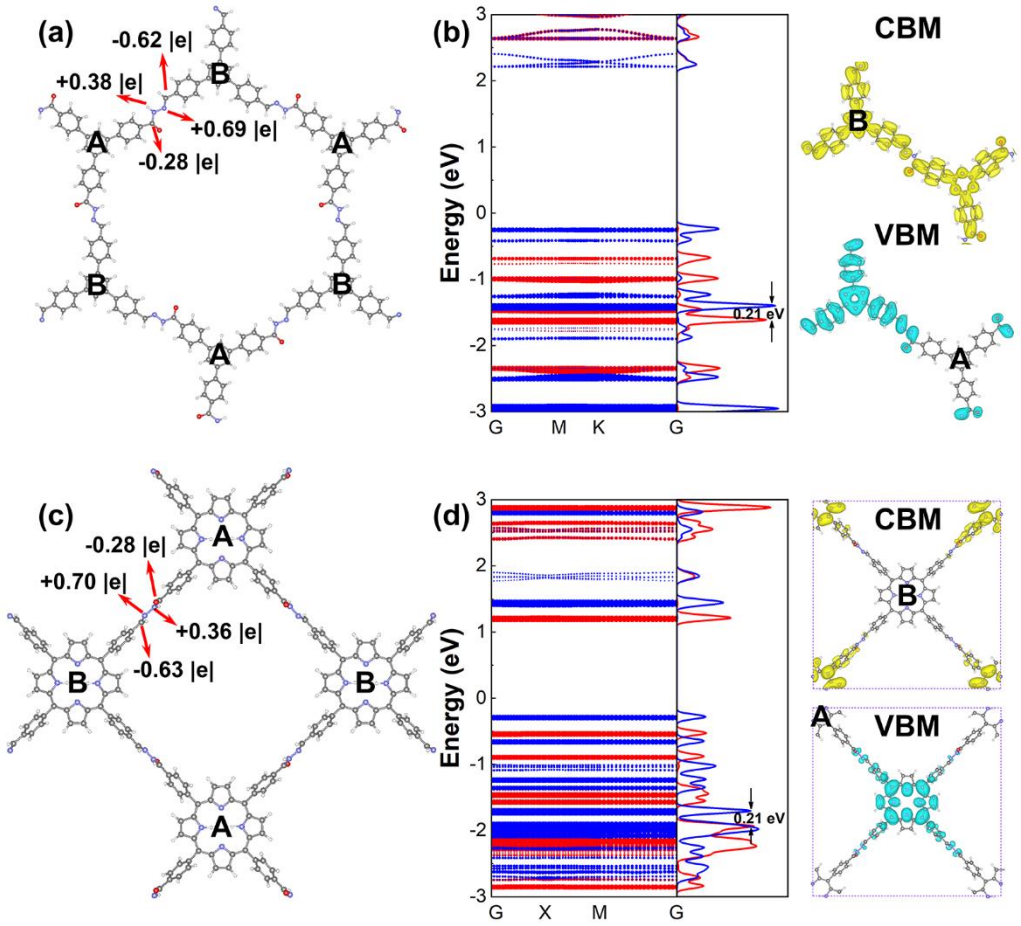

Figure S5. Optimized structures of (a) Hy-TPB and (c) Hy-TPP COFs monolayers, respectively, where C, N, H and O atoms are represented by gray, blue, white and red balls, respectively. Band structures of (b) Hy-TPB and (d) Hy-TPP projected onto the Core A (red) and Core B (blue) based on the PBE functional, respectively. The right column presents the decomposed charge densities of CBM and VBM. The yellow and bluish areas stand for the CBM and VBM with a contour surface of 0.004 |e|/Å^3.

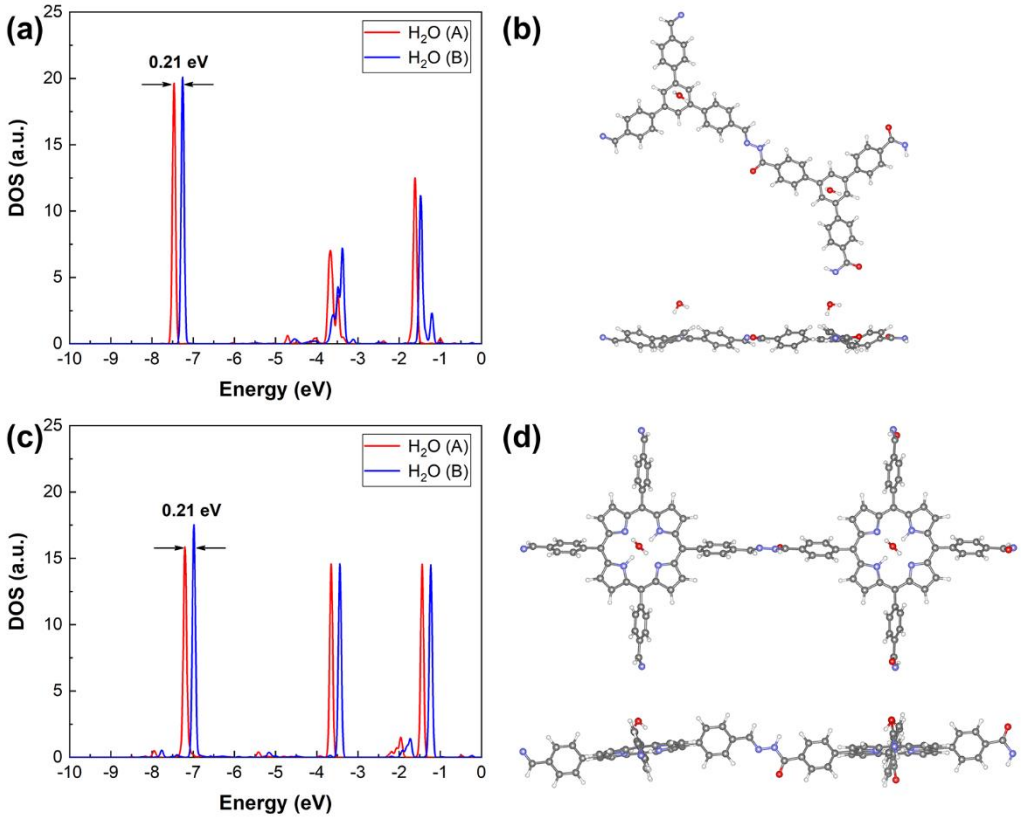

Figure S6. The projected DOS of H_2O molecules adsorbed on the Core A and Core B of (a) Hy-TPB and (c) Hy-TPP monolayers, respectively. The top and side views of H_2O molecules adsorbed on the Core A and Core B of (b) Hy-TPB and (d) Hy-TPP monolayers, respectively.

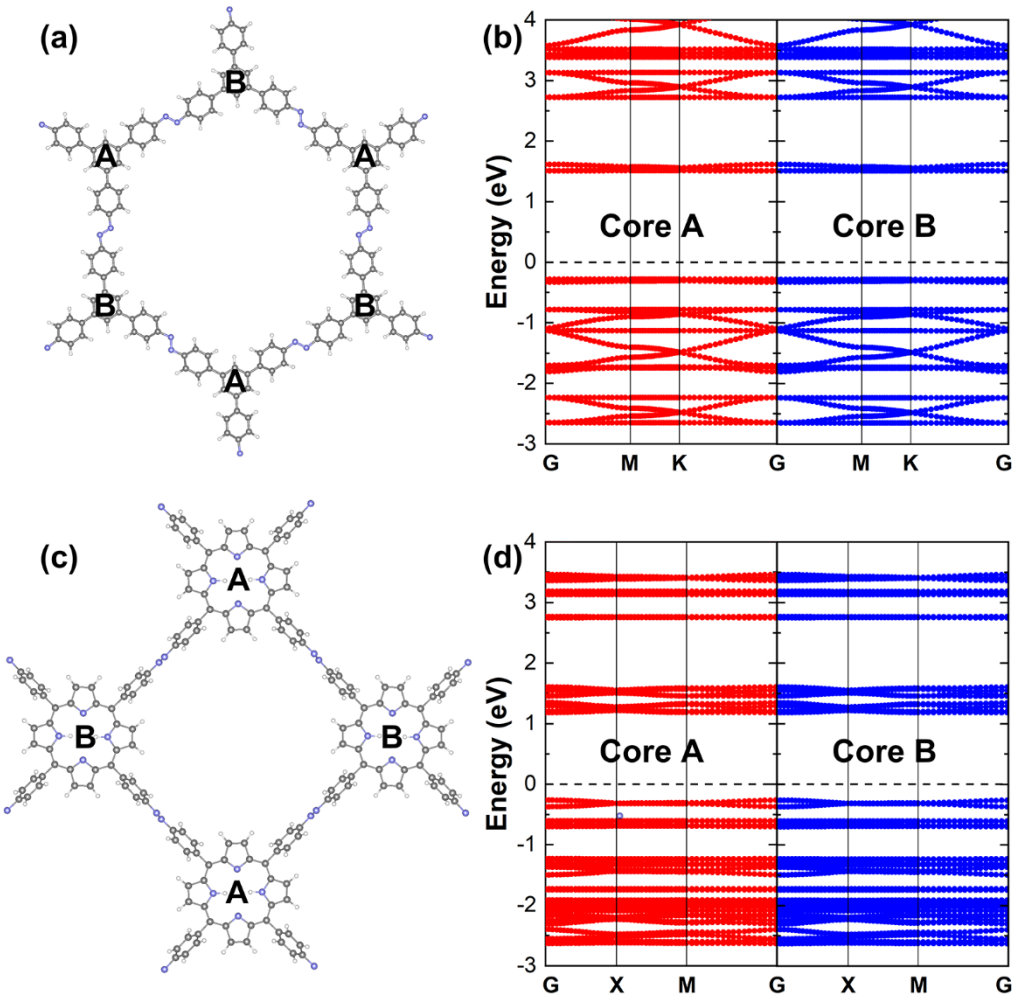

Figure S7. Optimized structures of (a) Azo-TPB and (c) Azo-TPP COFs monolayers, respectively, where C, N and H atoms are represented by gray, blue and white balls, respectively. Band structures of (b) Azo-TPB and (d) Azo-TPP projected onto the Core A (red) and Core B (blue) based on PBE functional, respectively, where the dashed lines stand for the fermi levels.

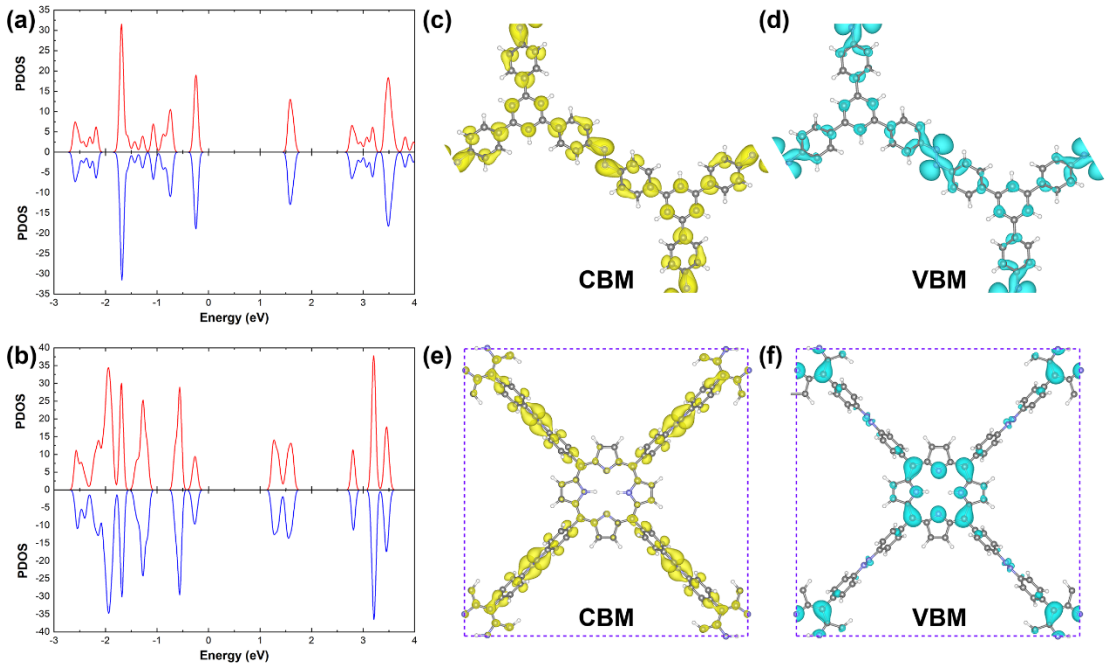

Figure S8. The projected DOS of Core A and Core B for (a) Azo-TPB and (b) Azo-TPP monolayers, respectively. The red and blue lines represent the Core A and Core B, respectively. The decomposed charge densities of (c) CBM and (d) VBM for the Azo-TPB. The decomposed charge densities of (e) CBM and (f) VBM for the Azo-TPP. The yellow and bluish areas stand for the CBM and VBM with a contour surface of 0.004 |e|/Å^3.

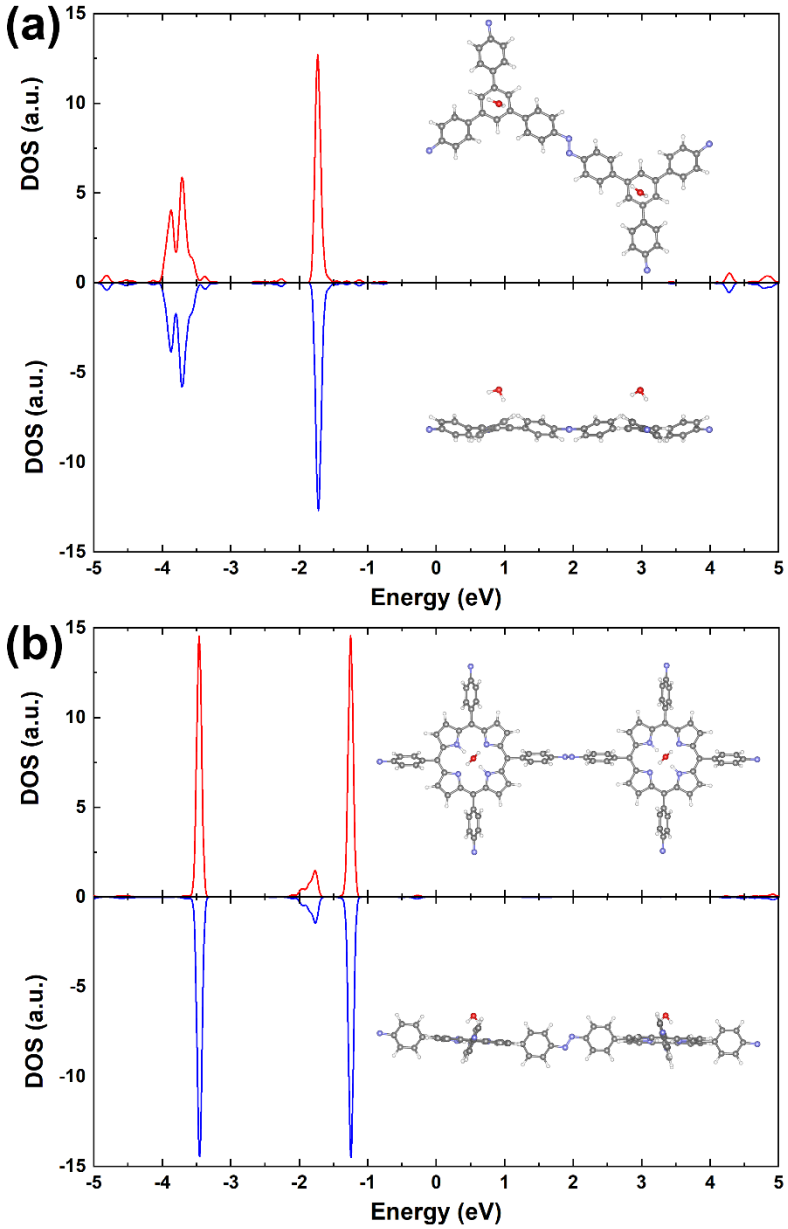

Figure S9. The projected DOS of H_2O molecules adsorbed on the Core A and Core B of (a) Azo-TPB and (b) Azo-TPP monolayers, respectively. The insets are the top and side views of H_2O molecules adsorbed on the Core A and Core B of Azo-TPB and Azo-TPP.

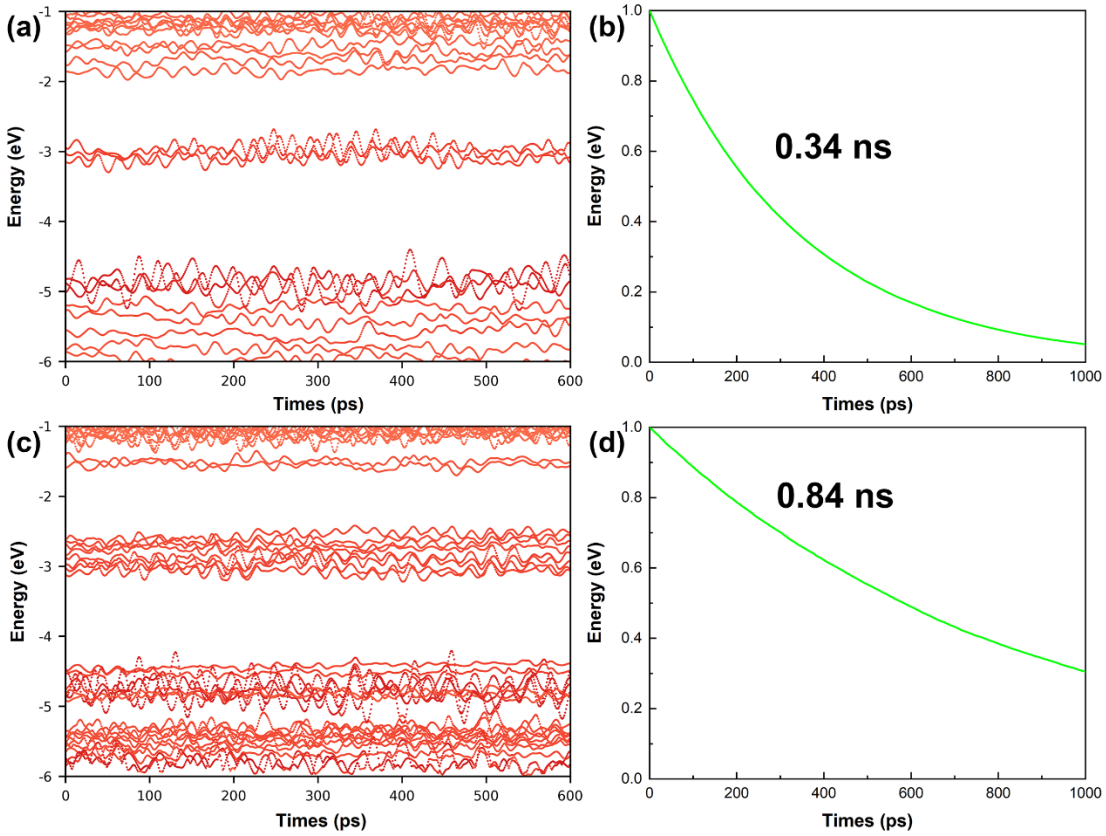

Figure S10. Time evolutions of energy levels in (a) Azo-TPB and (c) Azo-TPP, respectively. Dynamics of e–h recombination in (b) Azo-TPB and (d) Azo-TPP, respectively.

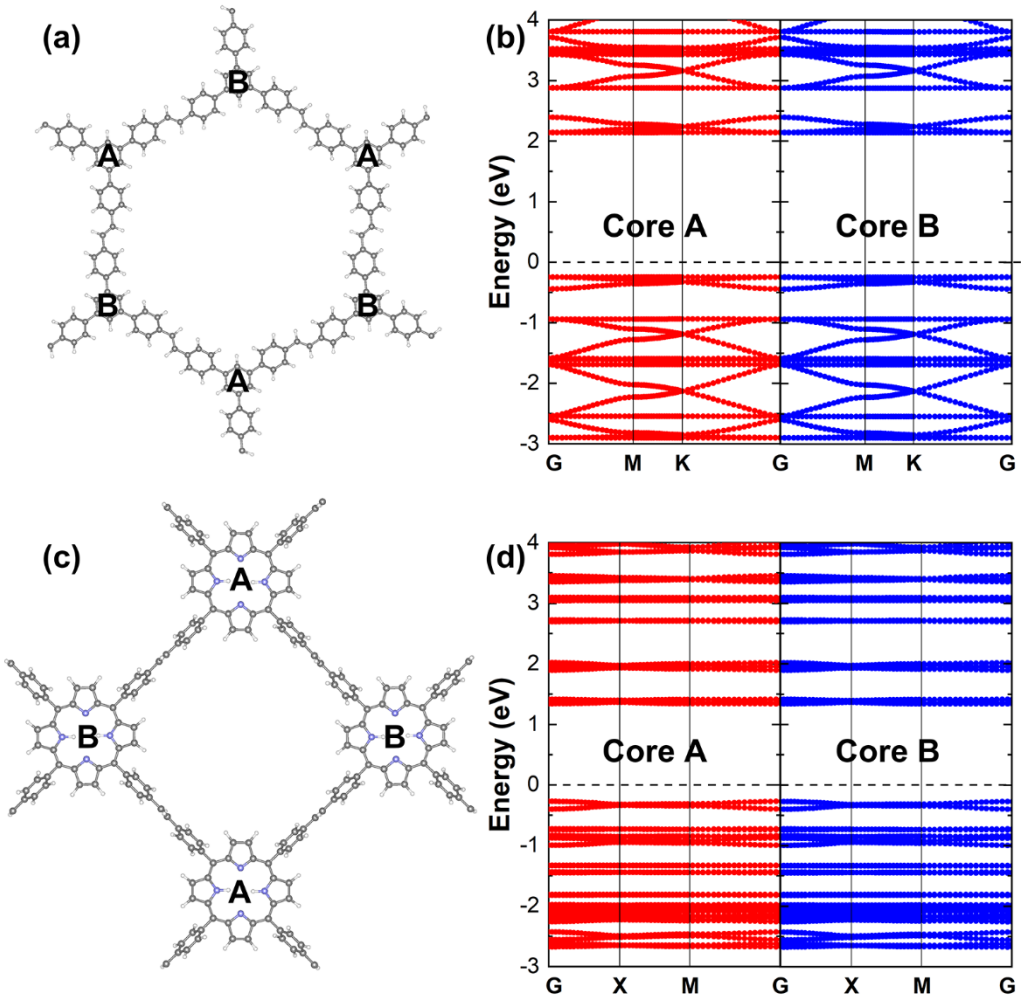

Figure S11. Optimized structures of (a) Olefin-TPB and (c) Olefin-TPP COFs monolayers, where C, N and H atoms are represented by gray, blue and white balls, respectively. Band structures of (b) Olefin-TPB and (d) Olefin-TPP projected onto the Core A (red) and Core B (blue) based on PBE functional, respectively, where the dashed lines stand for the fermi levels.

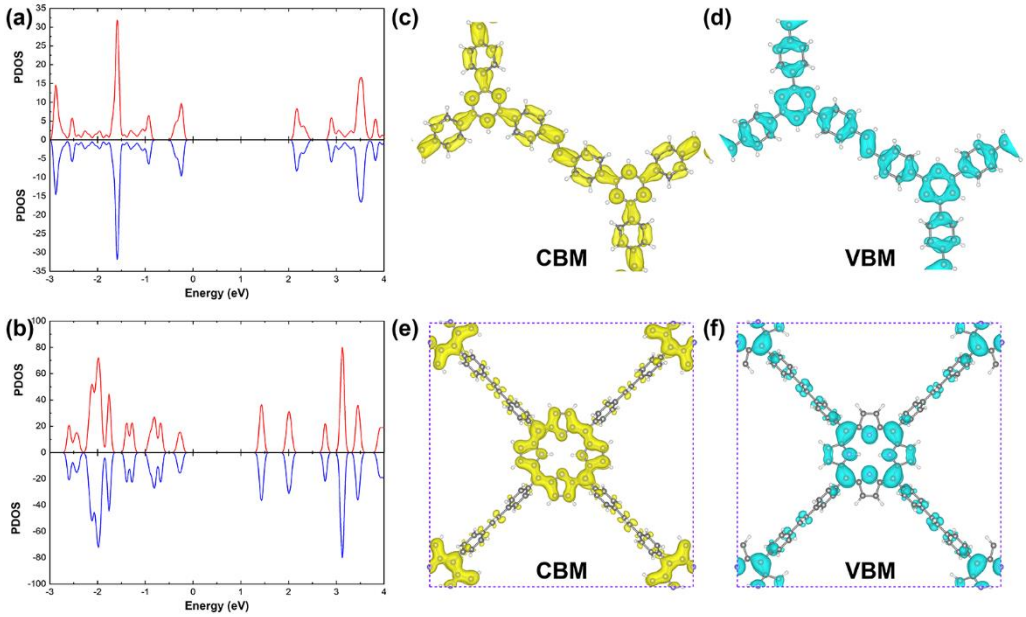

Figure S12. The projected DOS of Core A and Core B for (a) Olefin-TPB and (b) Olefin-TPP monolayers, respectively. The red and blue lines represent the Core A and Core B, respectively. The decomposed charge densities of (c) CBM and (d) VBM for the Olefin-TPB. The decomposed charge densities of (e) CBM and (f) VBM for the Olefin-TPP. The yellow and bluish areas stand for the CBM and VBM with a contour surface of 0.004 |e|/Å^3.

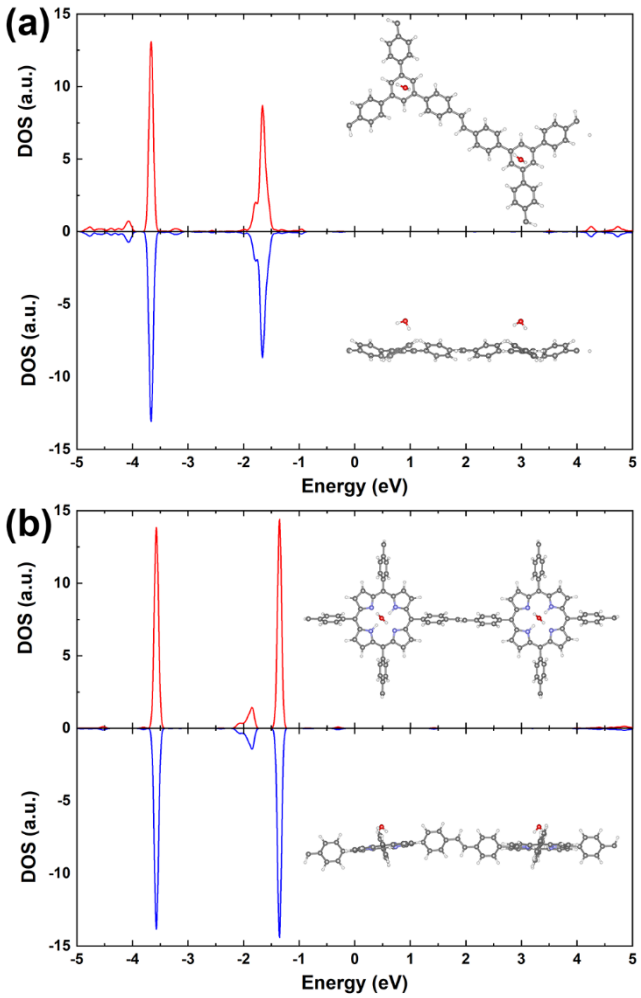

Figure S13. The projected DOS of H_2O molecules adsorbed on the Core A and Core B of (a) Olefin-TPB and (b) Olefin-TPP monolayers, respectively. The insets are the top and side views of H_2O molecules adsorbed on the Core A and Core B of Olefin-TPB and Olefin-TPP monolayers.

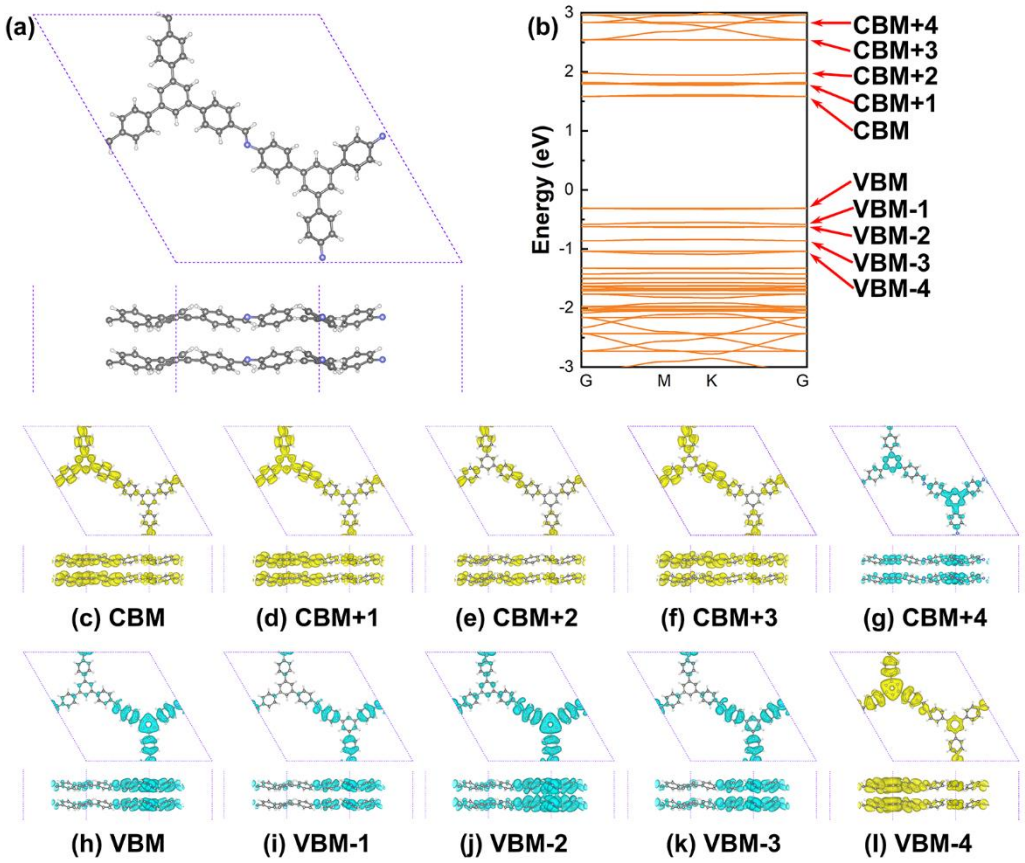

Figure S14. (a) Optimized structure and (b) calculated band structure of Im-TPB bilayer with AA stacking pattern based on PBE function, respectively. (c-i) Decomposed charge densities of the energy levels near CBM and VBM. The yellow and bluish areas stand for the Core A and Core B with a contour surface of 0.004 |e|/Å^3.

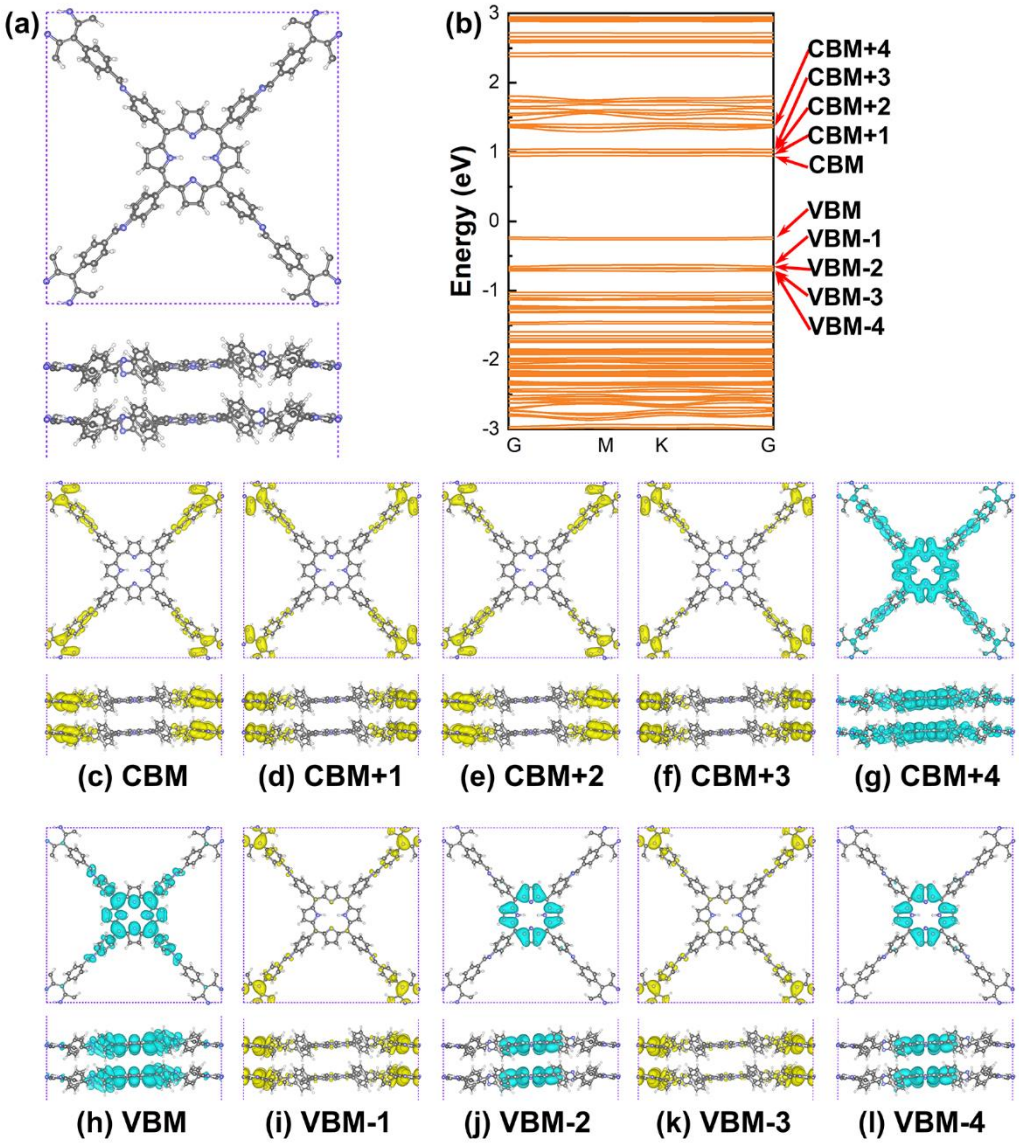

Figure S15. (a) Optimized structure and (b) calculated band structure of Im-TPP bilayer with AA stacking pattern based on PBE function, respectively. (c-i) Decomposed charge densities of the energy levels near CBM and VBM. The yellow and bluish areas stand for the Core A and Core B with a contour surface of 0.004 |e|/Å^3.

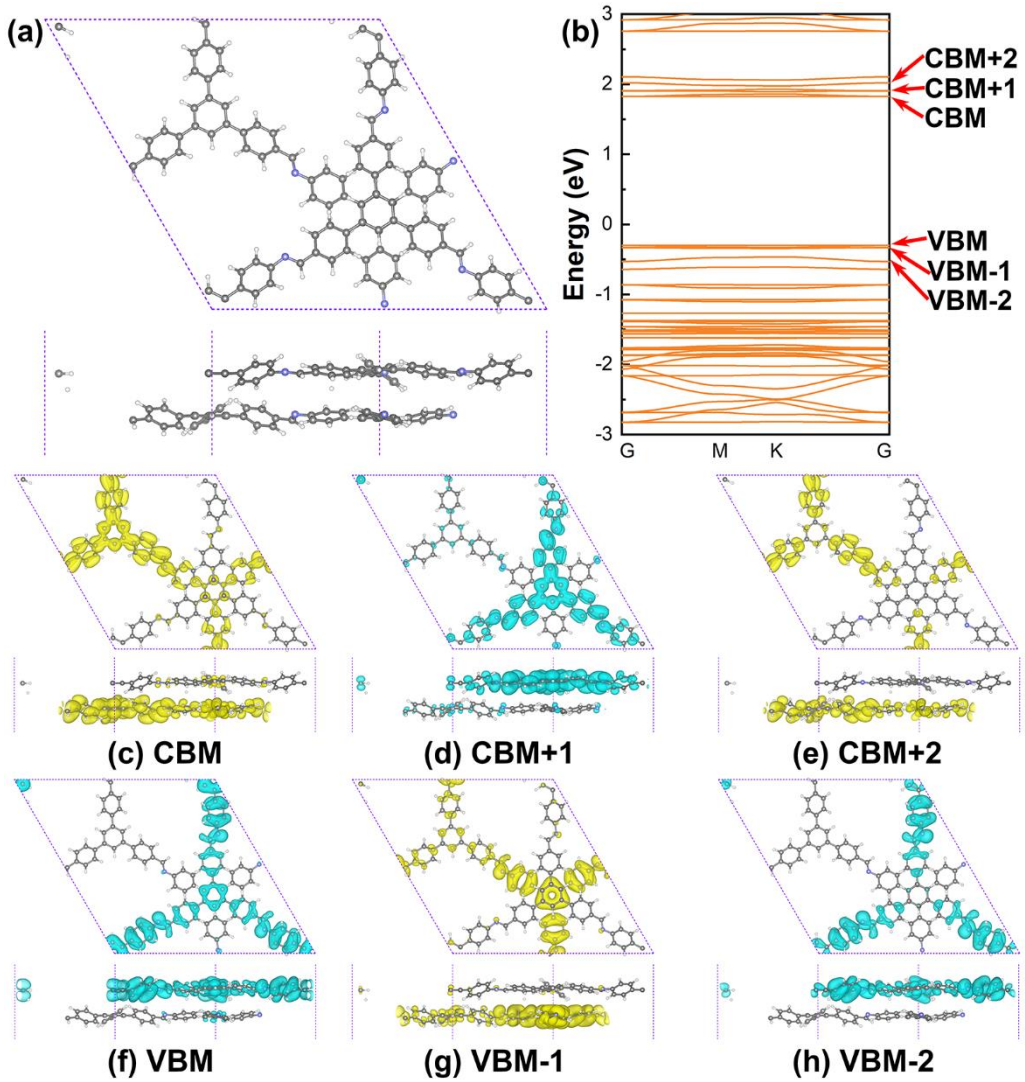

Figure S16. (a) Optimized structure and (b) calculated band structure of Im-TPB bilayer with AB stacking pattern based on PBE function, respectively. (c-h) Decomposed charge densities of the energy levels near CBM and VBM. The yellow and bluish areas stand for the bottom layer and top layer with a contour surface of 0.004 |e|/Å^3.

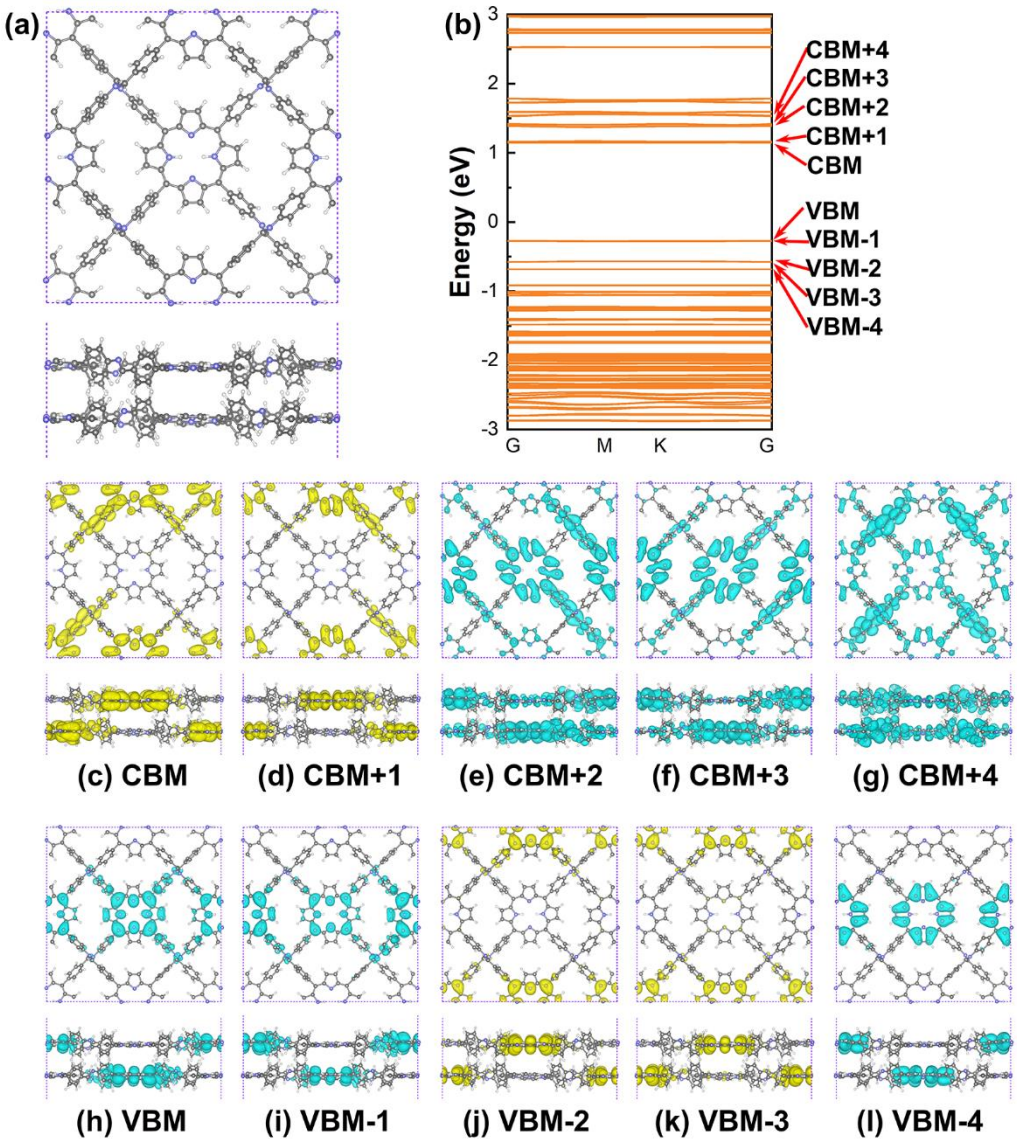

Figure S17. (a) Optimized structure and (b) calculated band structure of Im-TPP bilayer with a sliding pattern based on PBE function, respectively. (c-i) Decomposed charge densities of the energy levels near CBM and VBM. The yellow and bluish areas stand for the Core A and Core B with a contour surface of 0.004 |e|/Å^3.

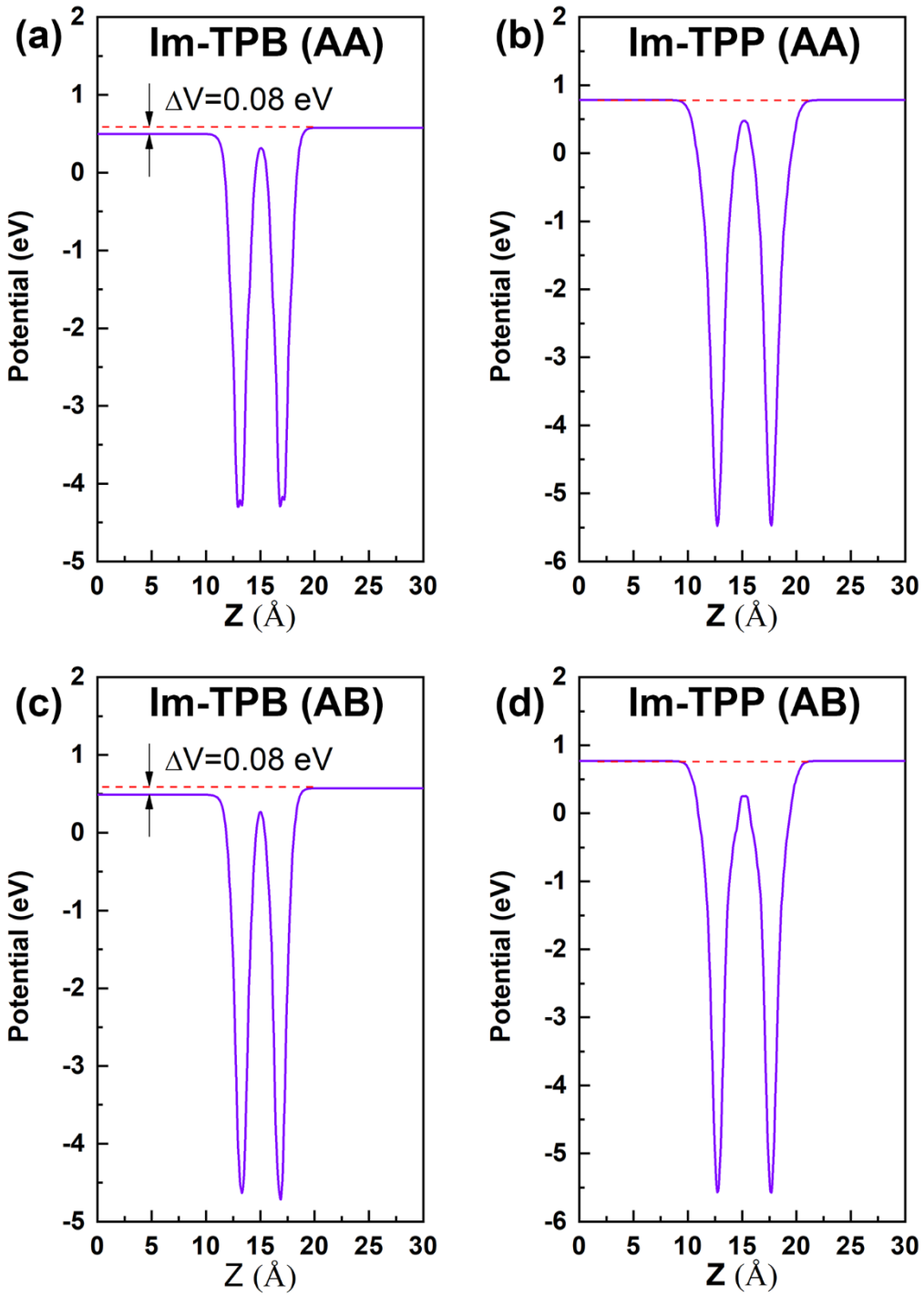

Figure S18. Plane-averaged electrostatic potential difference along the vertical direction for (a) AA-stacked Im-TPB bilayer, (b) AA-stacked Im-TPP bilayer, (c) AB-stacked Im-TPB bilayer and (d) Im-TPP bilayer with sliding pattern, respectively.

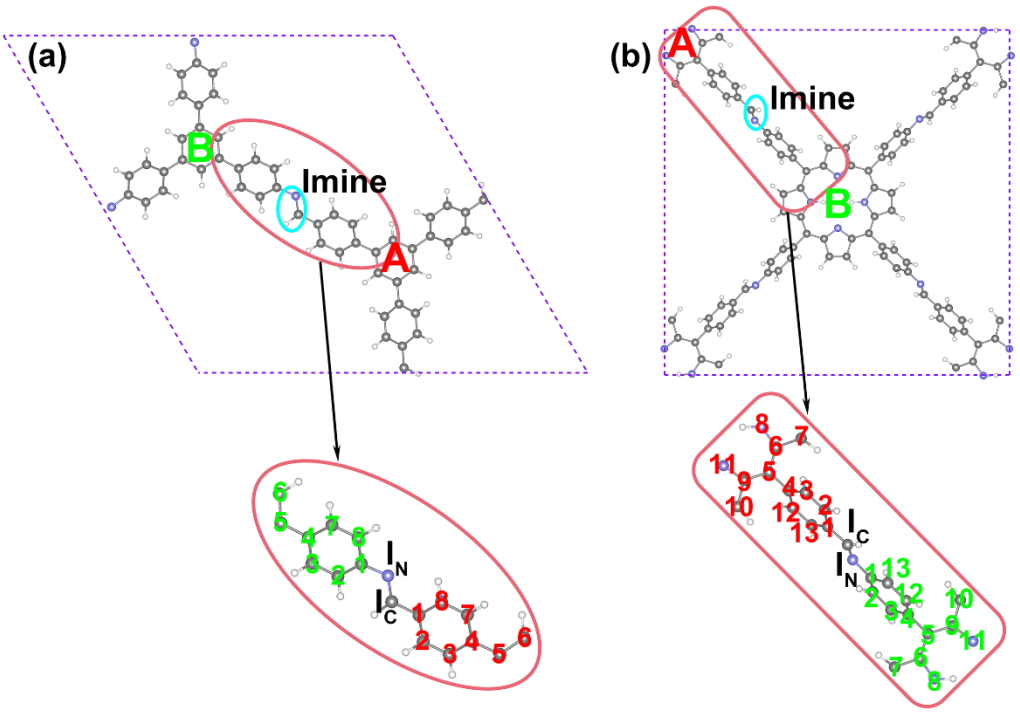

Figure S19. The selected active sites of (a) Im-TPB and (b) Im-TPP, respectively.

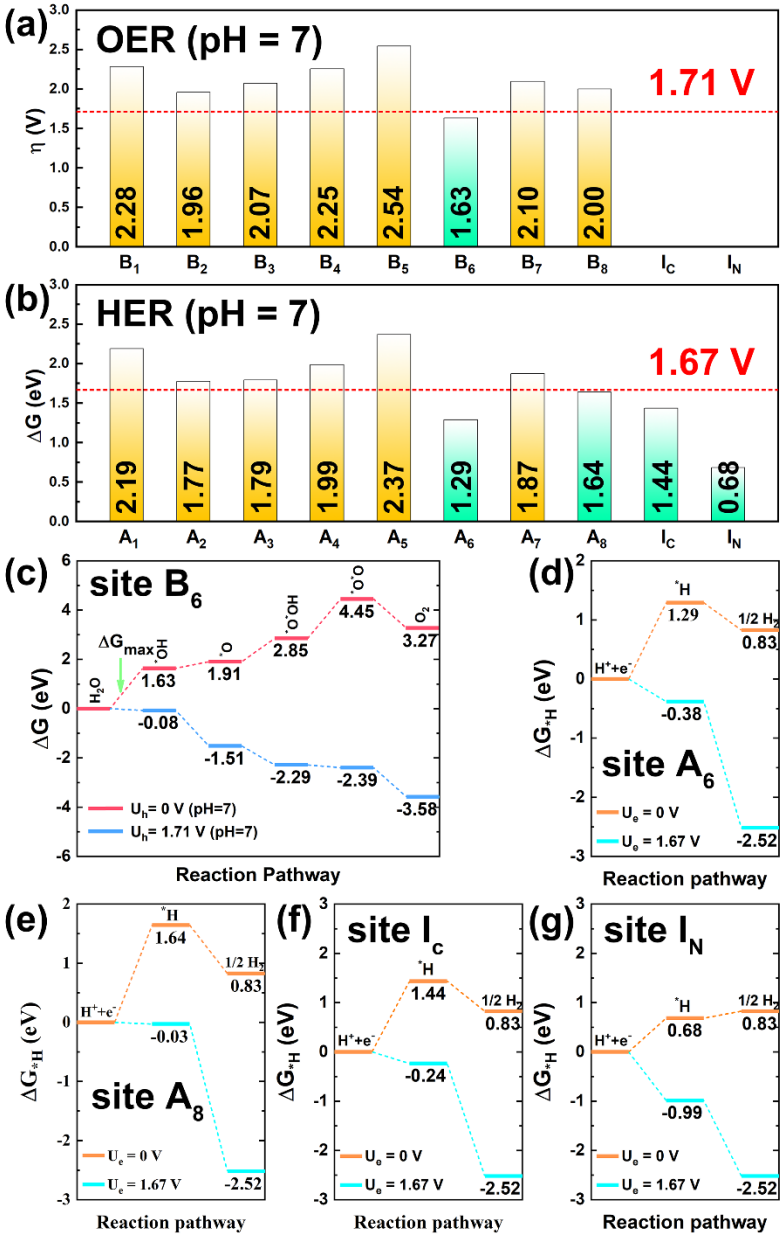

Figure S20. Overpotentials of OER (a) and (b) HER for the Im-TPB at pH = 7, respectively. The red dotted line in (a) indicates the U_h of 1.71 V. The red dotted line in (b) indicates the U_e of 1.67 V. (c) Free energy diagram of Im-TPB for OER process occurred at site B_6. Free energy diagram of Im-TPB for HER process occurred at (d) site A_6, (e) site A_8, (f) site I_C and (g) site I_N, respectively.

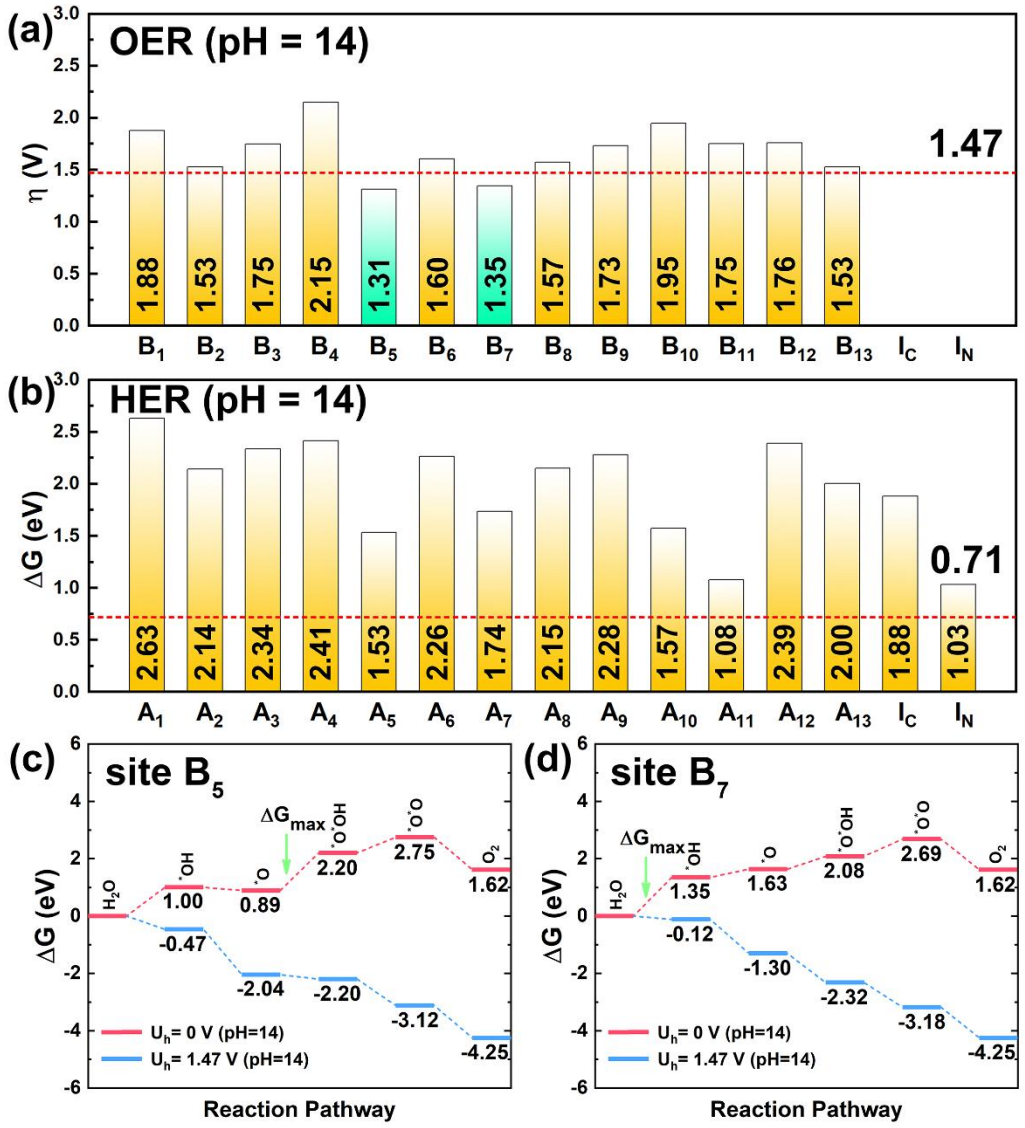

Figure S21. Overpotentials of OER (a) and (b) HER for the Im-TPP at pH = 14, respectively. The red dotted line in (a) indicates the U_h of 1.47 V. The red dotted line in (b) indicates the U_e of 0.71 V. Free energy diagram of Im-TPP for OER process occurred at (c) site B_6 and (d) site B_7, respectively.

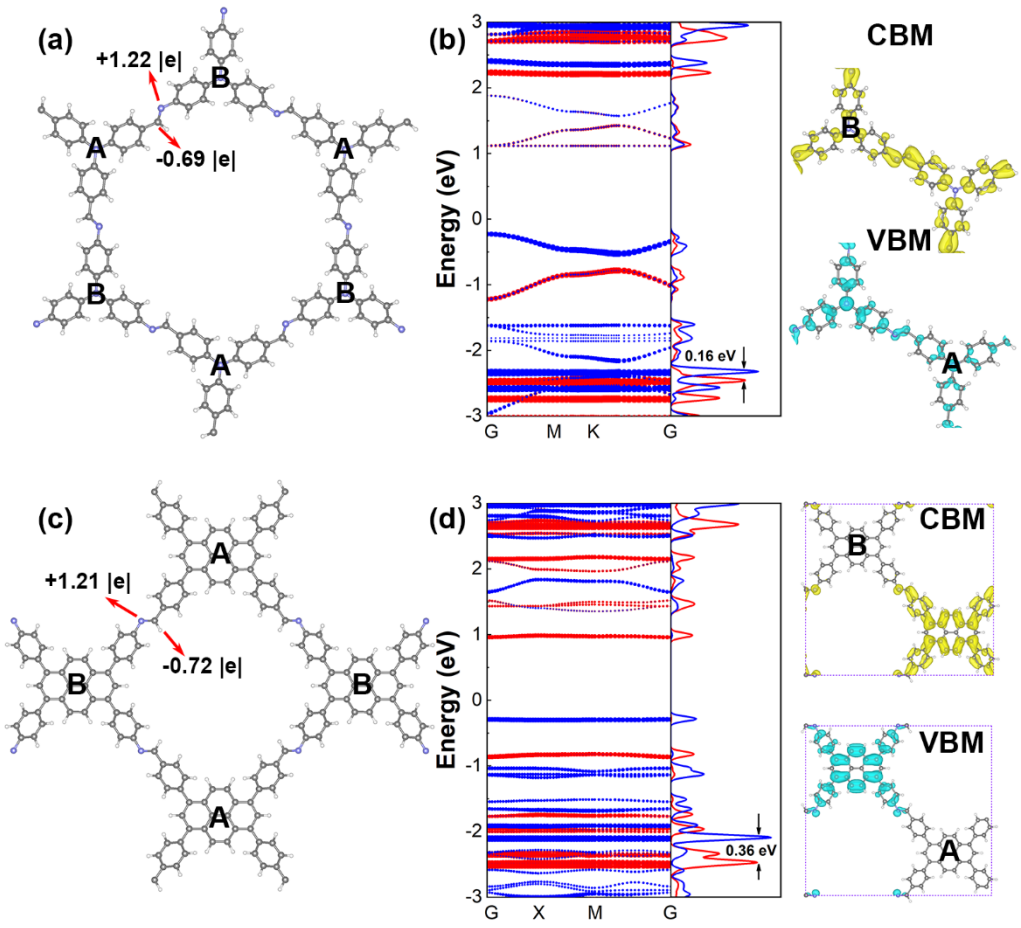

Figure S22. Optimized structures of (a) Im-TPA and (c) Im-PTT COFs monolayers, respectively, where C, N and H atoms are represented by gray, blue and white balls, respectively. Band structures of (b) Im-TPA and (d) Im-PTT projected onto the Core A (red) and Core B (blue) based on the PBE functional, respectively. The right column presents the decomposed charge densities of CBM and VBM. The yellow and bluish areas stand for the CBM and VBM with a contour surface of 0.004 |e|/Å^3.

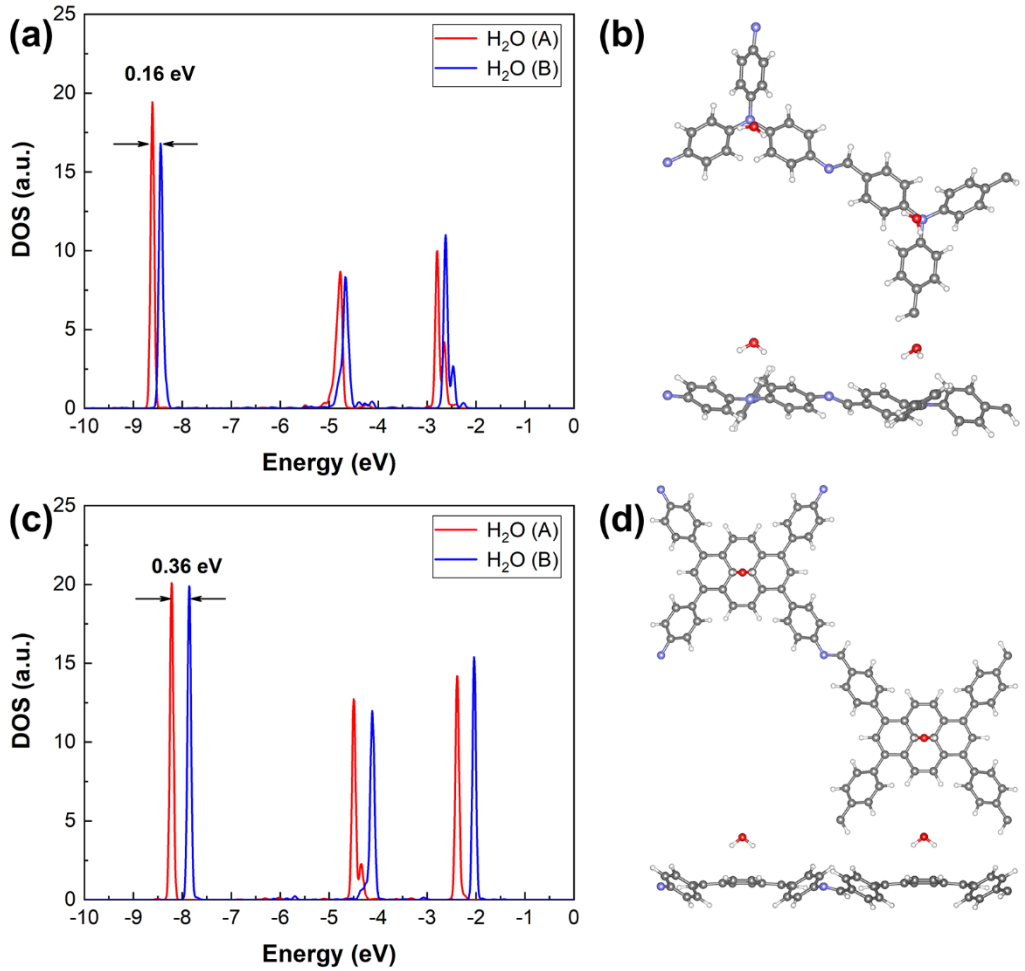

Figure S23. The projected DOS of H_2O molecules adsorbed on the Core A and Core B of (a) Im-TPA and (c) Im-PTT monolayers, respectively. The top and side views of H_2O molecules adsorbed on the Core A and Core B of (b) Im-TPA and (d) Im-PTT monolayers, respectively.

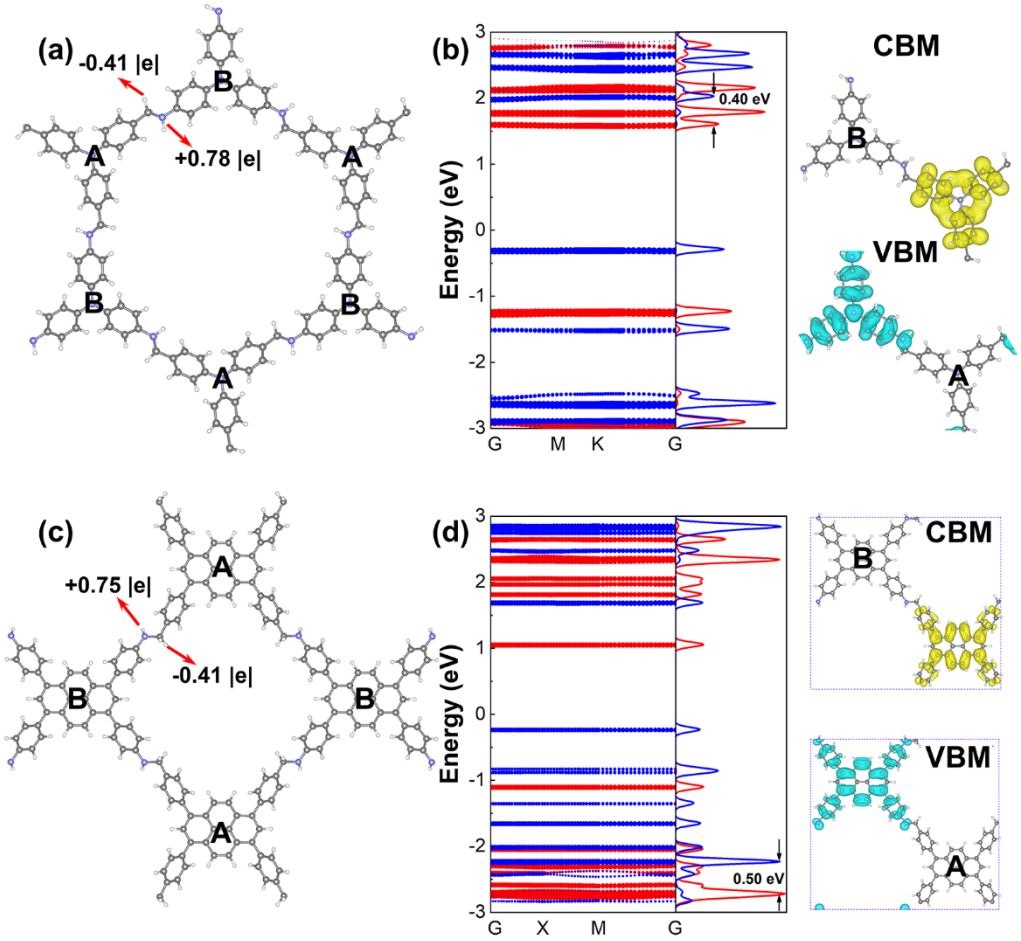

Figure S24. Optimized structures of (a) Am-TPA and (c) Am-PTT COFs monolayers, respectively, where C, N and H atoms are represented by gray, blue and white balls, respectively. Band structures of (b) Am-TPA and (d) Am-PTT projected onto the Core A (red) and Core B (blue) based on the PBE functional, respectively. The right column presents the decomposed charge densities of CBM and VBM. The yellow and bluish areas stand for the CBM and VBM with a contour surface of 0.004 |e|/Å^3.

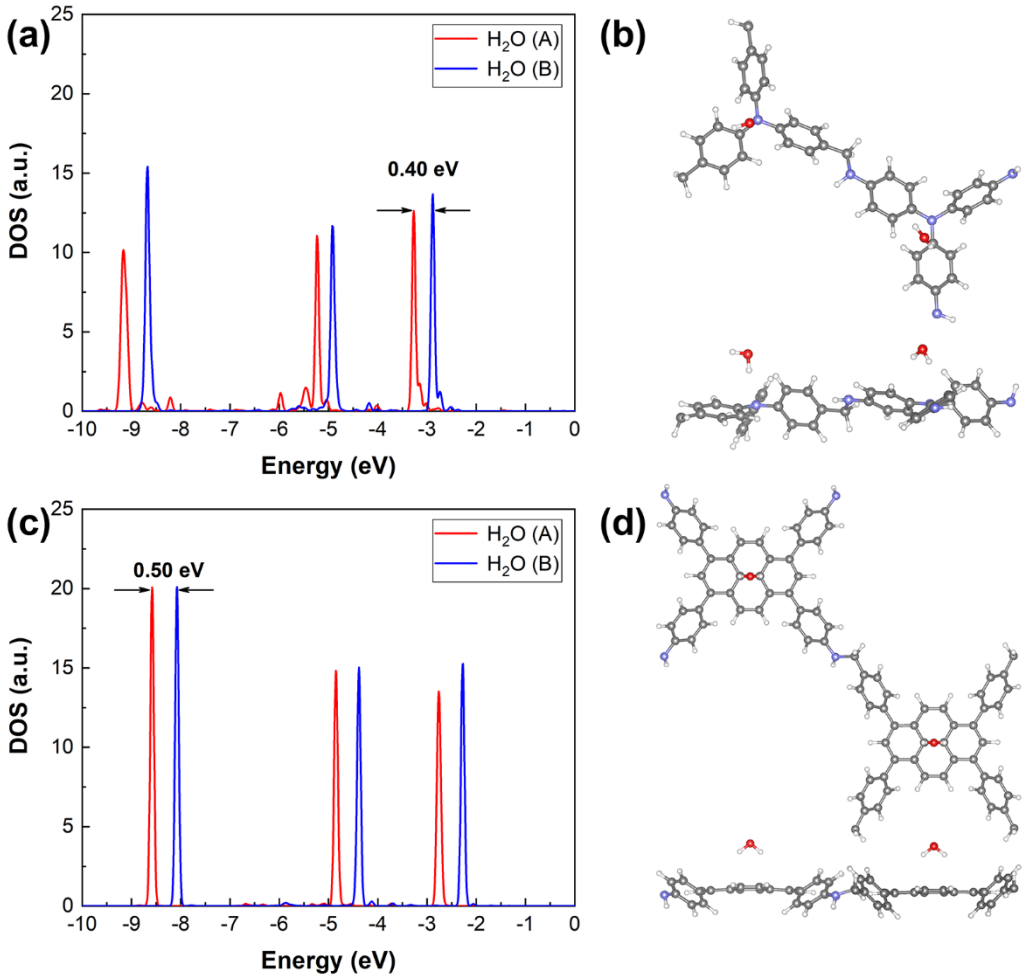

Figure S25. The projected DOS of H_2O molecules adsorbed on the Core A and Core B of (a) Am-TPA and (c) Am-PTT monolayers, respectively. The top and side views of H_2O molecules adsorbed on the Core A and Core B of (b) Am-TPA and (d) Am-PTT monolayers, respectively.

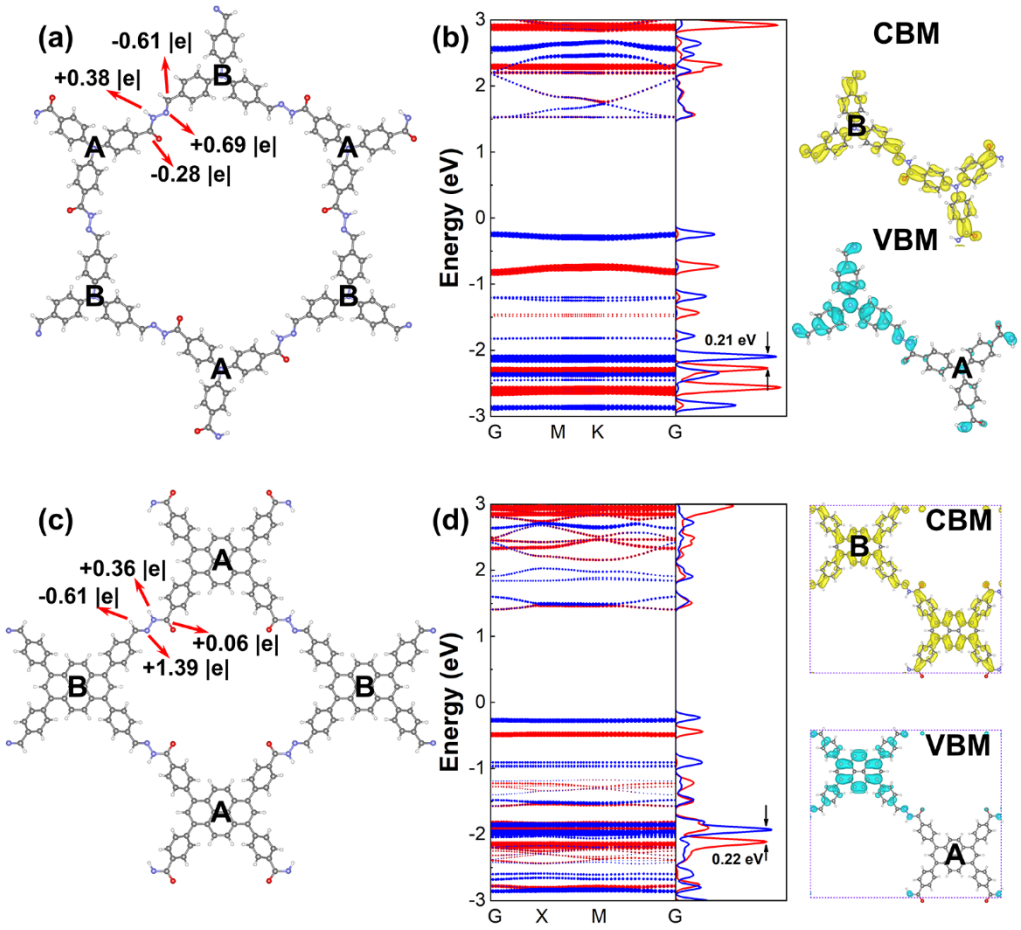

Figure S26. Optimized structures of (a) Hy-TPA and (c) Hy-PTT COFs monolayers, respectively, where C, N, H and O atoms are represented by gray, blue, white and red balls, respectively. Band structures of (b) Hy-TPA and (d) Hy-PTT projected onto the Core A (red) and Core B (blue) based on the PBE functional, respectively. The right column presents the decomposed charge densities of CBM and VBM. The yellow and bluish areas stand for the CBM and VBM with a contour surface of 0.004 |e|/Å^3.

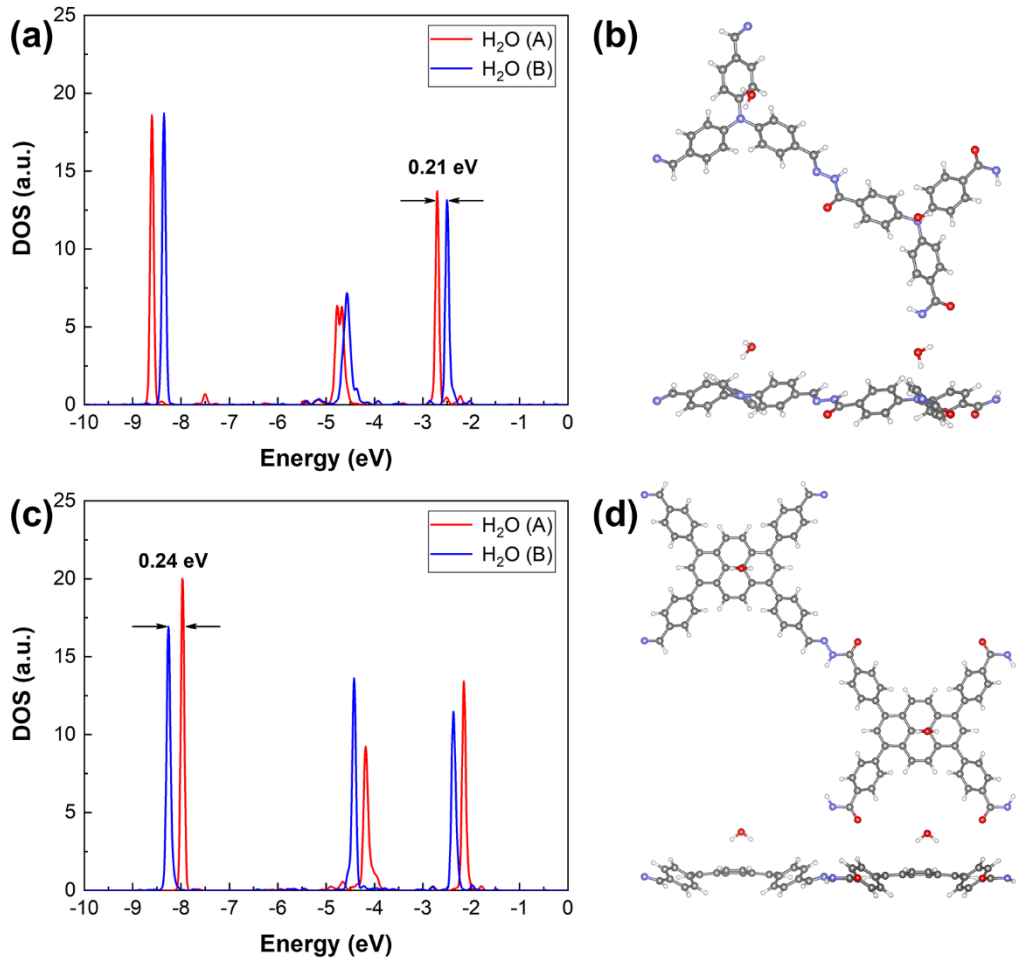

Figure S27. The projected DOS of H_2O molecules adsorbed on the Core A and Core B of (a) Hy-TPA and (c) Hy-PTT monolayers, respectively. The top and side views of H_2O molecules adsorbed on the Core A and Core B of (b) Hy-TPA and (d) Hy-PTT monolayers, respectively.

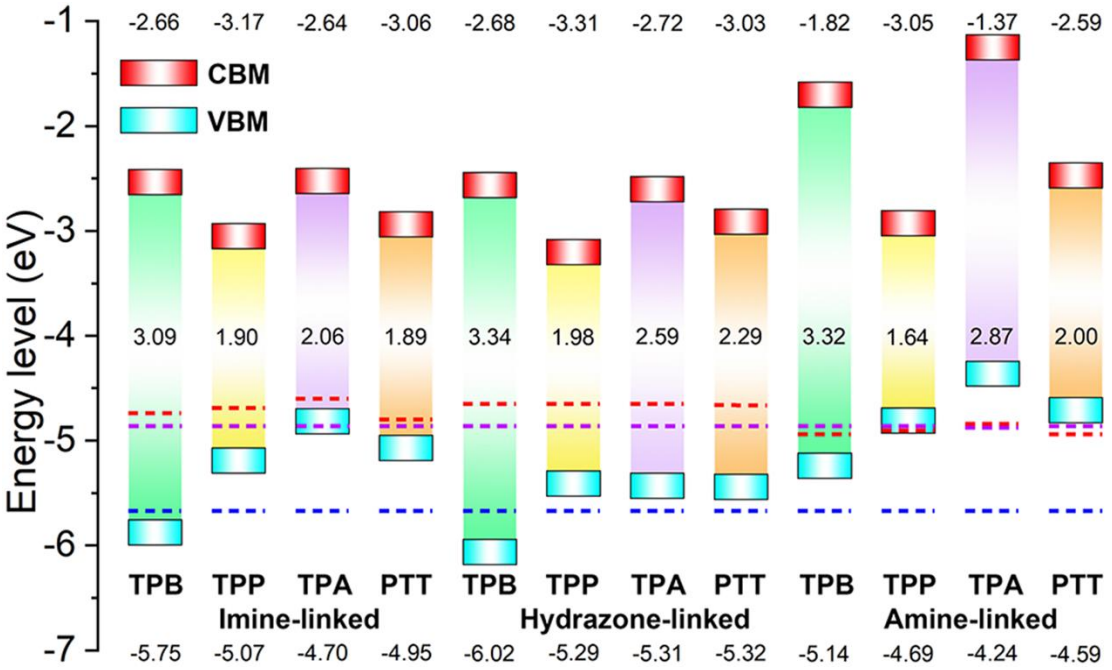

Figure S28. The calculated energy positions of VBM and CBM of polarized-bond-linked COFs monolayers relative to vacuum level based on the HSE06 functional. The red and blue dashed lines represent the hydrogen reduction potential and water oxidation potential at pH = 0, respectively. The purple dashed lines are water oxidation potential at pH = 14.

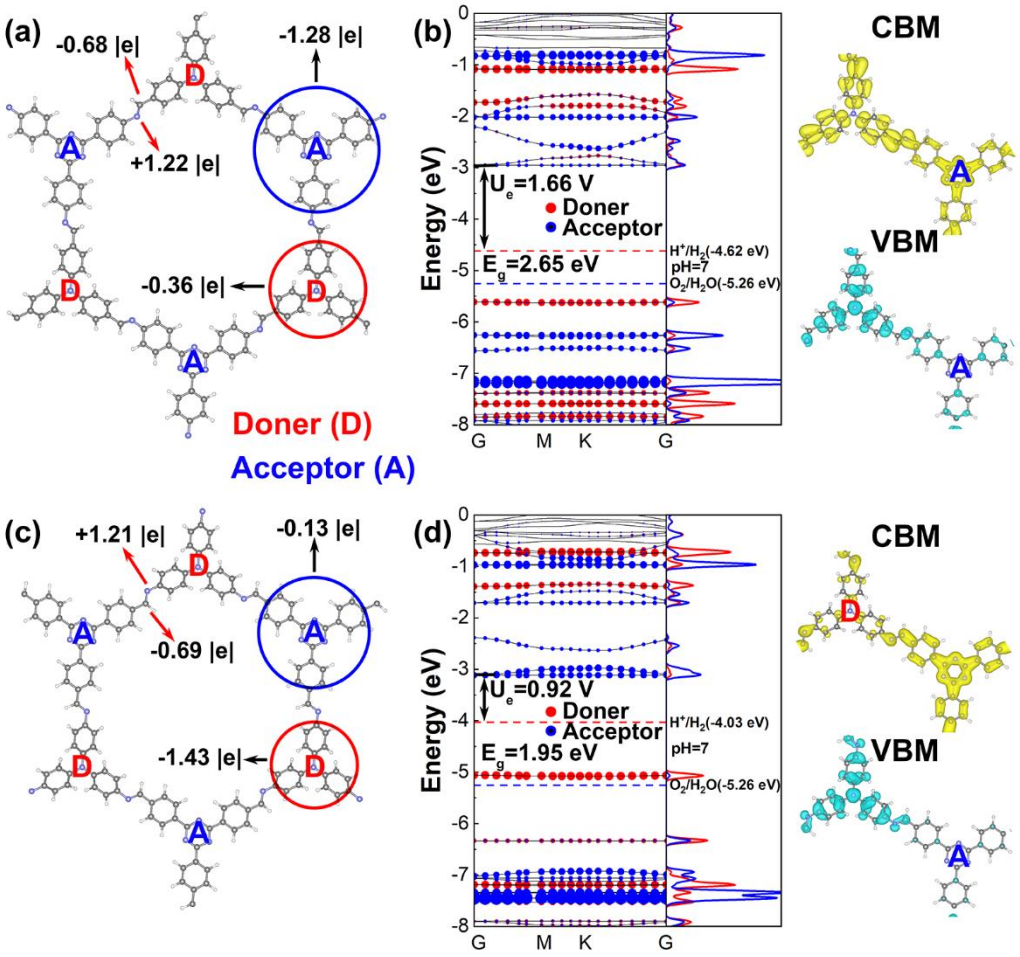

Figure S29. Optimized structures of (a) DCNA-1 and (c) DNCA-1 COFs monolayers, respectively, where C, N and H atoms are represented by gray, blue and white balls, respectively. Band structures of (b) DCNA-1 and (d) DNCA-1 projected onto the D (red) and A (blue) moieties based on the HSE06 functional, respectively. The right column presents the decomposed charge densities of CBM and VBM. The yellow and bluish areas stand for the CBM and VBM with a contour surface of 0.004 |e|/Å^3.

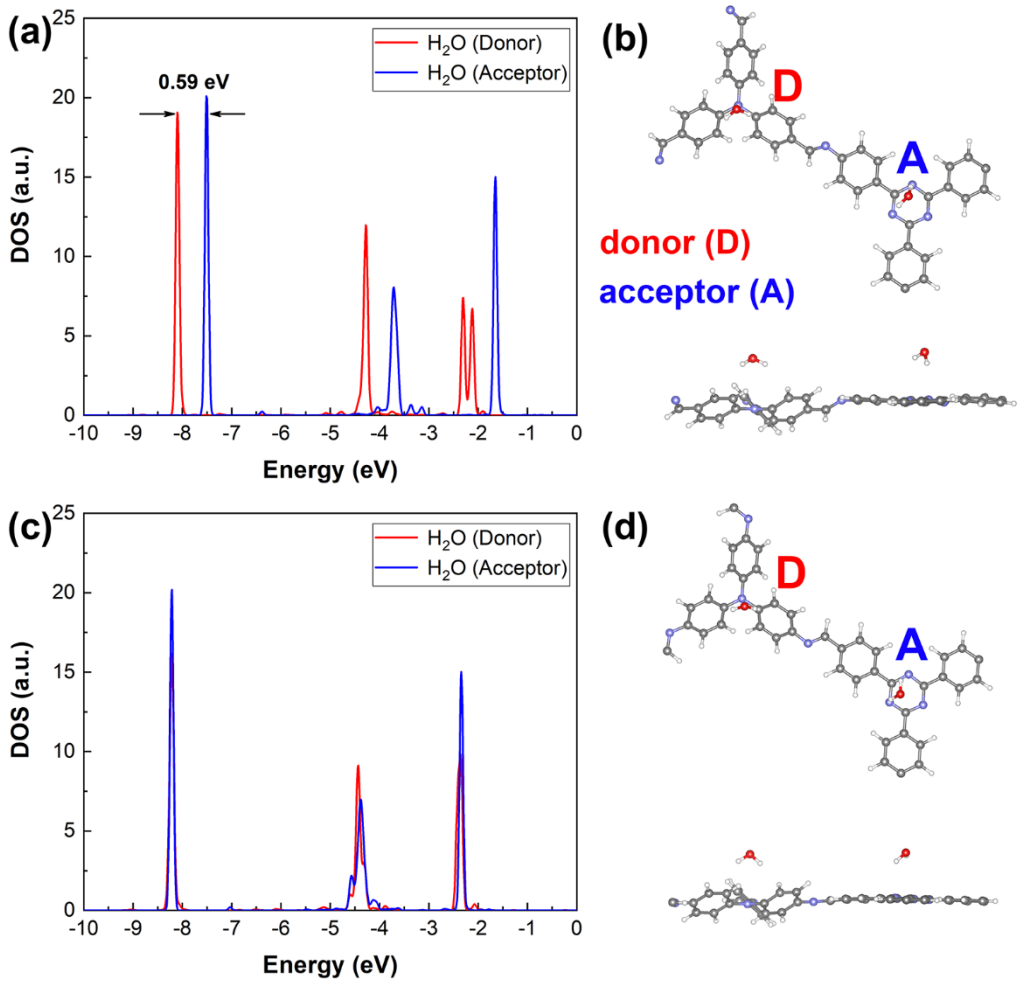

Figure S30. The projected DOS of H_2O molecules adsorbed on the Core A and Core B of (a) DCNA-1 and (c) DNCA-1 COFs monolayers, respectively. The top and side views of H_2O molecules adsorbed on the Core A and Core B of (b) DCNA-1 and (d) DNCA-1 COFs monolayers, respectively.

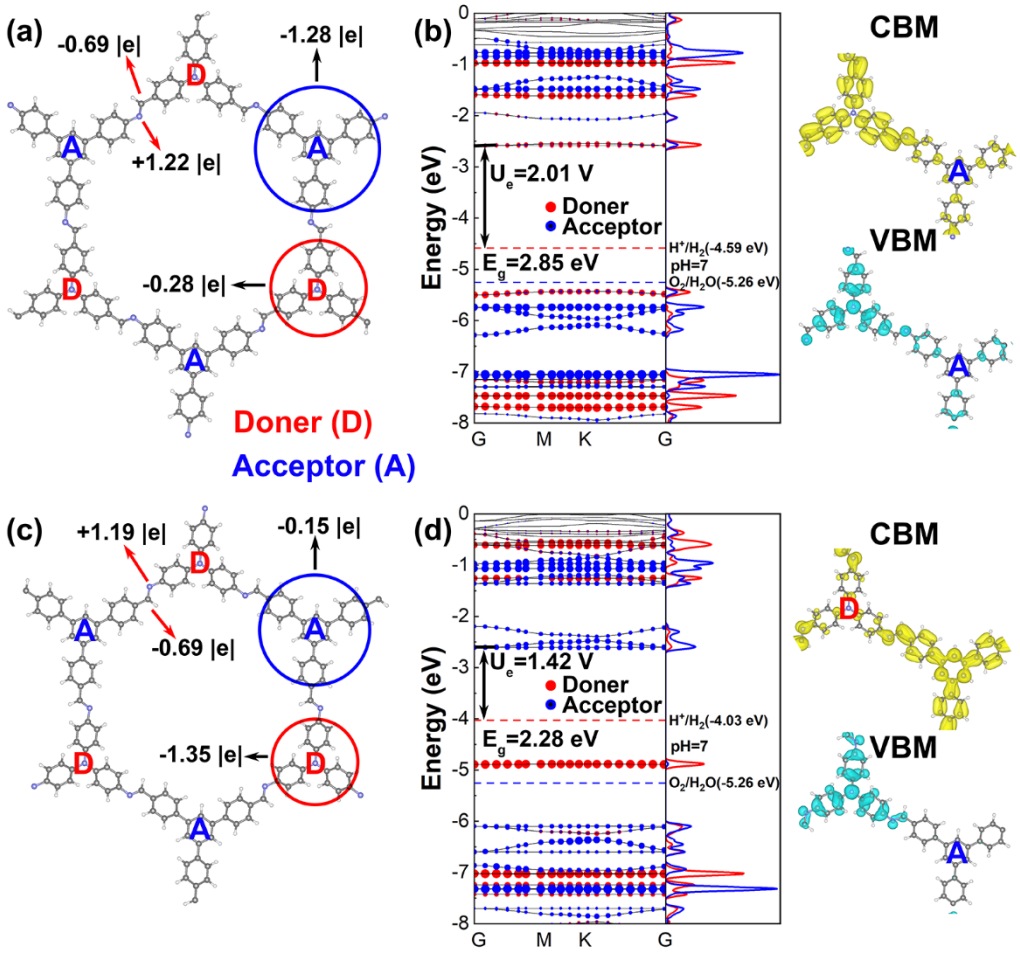

Figure S31. Optimized structures of (a) DCNA-2 and (c) DNCA-2 COFs monolayers, respectively, where C, N and H atoms are represented by gray, blue and white balls, respectively. Band structures of (b) DCNA-2 and (d) DNCA-2 projected onto the D (red) and A (blue) moieties based on the HSE06 functional, respectively. The right column presents the decomposed charge densities of CBM and VBM. The yellow and bluish areas stand for the CBM and VBM with a contour surface of 0.004 |e|/Å^3.

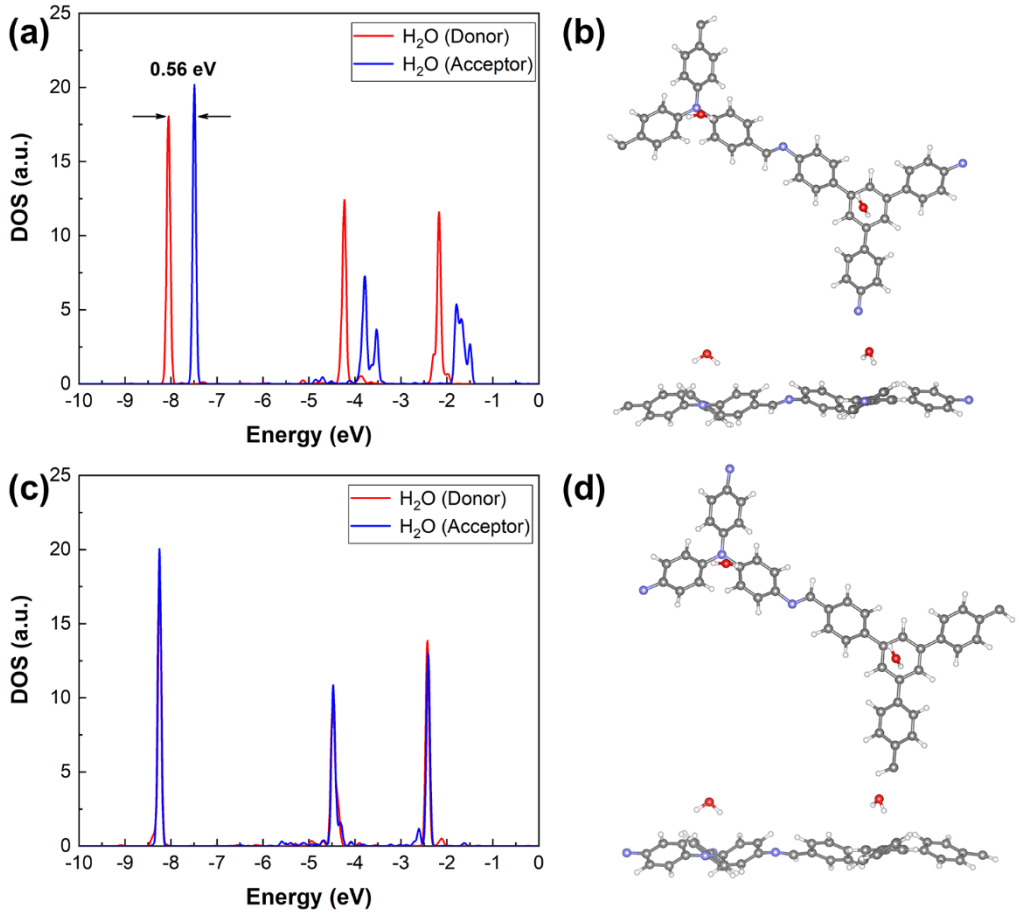

Figure S32. The projected DOS of H_2O molecules adsorbed on the Core A and Core B of (a) DCNA-2 and (c) DNCA-2 COFs monolayers, respectively. The top and side views of H_2O molecules adsorbed on the Core A and Core B of (b) DCNA-2 and (d) DNCA-2 COFs monolayers, respectively.

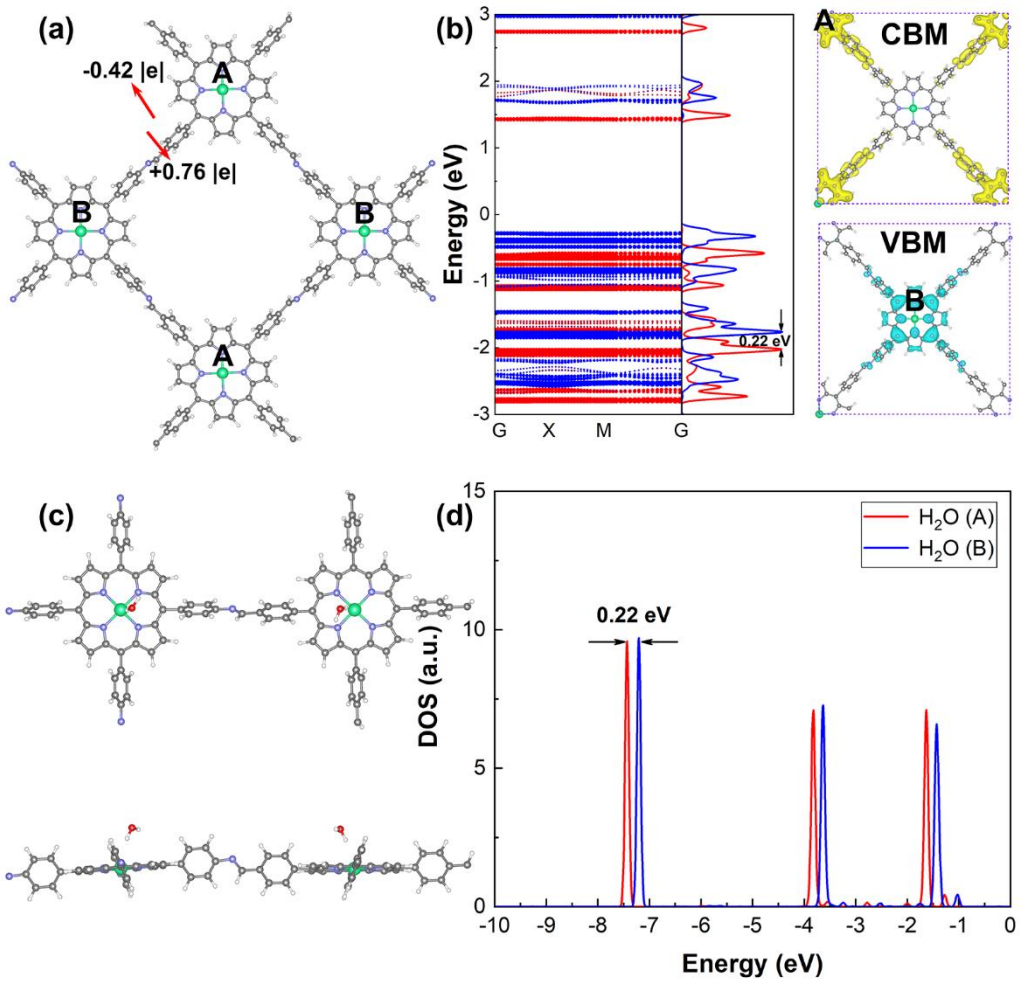

Figure S33. (a) Optimized structures of Pt-embedded Im-TPP monolayer, where C, N, H and Pt atoms are represented by gray, blue, white and green balls, respectively. (b) Band structures of Pt-embedded Im-TPP projected onto the Core A (red) and Core B (blue) based on the PBE functional. The right column presents the decomposed charge densities of CBM and VBM. The yellow and bluish areas stand for the CBM and VBM with a contour surface of 0.004 |e|/Å^3. (c) The top and side views of H_2O molecules adsorbed on the Core A and Core B of Pt-embedded Im-TPP monolayer. (d) The projected DOS of H_2O molecules adsorbed on the Core A and Core B of Pt-embedded Im-TPP monolayer.

REFERENCES

1. Zheng, Q.; Chu, W.; Zhao, C.; Zhang, L.; Guo, H.; Wang, Y.; Jiang, X.; Zhao, J., Ab initio nonadiabatic molecular dynamics investigations on the excited carriers in condensed matter systems. *WIRES Comput. Mol. Sci.* **2019,** *9* (6), e1411.

2. Craig, C. F.; Duncan, W. R.; Prezhdo, O. V., Trajectory surface hopping in the time-dependent Kohn-Sham approach for electron-nuclear dynamics. *Phys. Rev. Lett.* **2005,** *95* (16), 163001.

3. Jaeger, H. M.; Fischer, S.; Prezhdo, O. V., Decoherence-induced surface hopping. *J. Chem. Phys.* **2012,** *137* (22), 22A545.

4. Tully, J. C., Molecular dynamics with electronic transitions. *J. Chem. Phys.* **1990,** *93* (2), 1061-1071.

5. Gajdoš, M.; Hummer, K.; Kresse, G.; Furthmüller, J.; Bechstedt, F., Linear optical properties in the projector-augmented wave methodology. *Phys. Rev. B* **2006,** *73* (4), 045112.

6. Nørskov, J. K.; Rossmeisl, J.; Logadottir, A.; Lindqvist, L., Origin of the Overpotential for Oxygen Reduction at a Fuel-Cell Cathode. *J. Phys. Chem. B* **2004,** *108*, 17886-17892.

7. Greeley, J.; Jaramillo, T. F.; Bonde, J.; Chorkendorff, I. B.; Norskov, J. K., Computational high-throughput screening of electrocatalytic materials for hydrogen evolution. *Nat. Mater.* **2006,** *5* (11), 909-13.

8. Rossmeisl, J.; Qu, Z. W.; Zhu, H.; Kroes, G. J.; Nørskov, J. K., Electrolysis of water on oxide surfaces. *J. Electroanal. Chem.* **2007,** *607*, 83-89.

9. Valde´s, A.; Qu, Z.-W.; Kroes, G.-J., Oxidation and Photo-Oxidation of Water on TiO_2 Surface. *J. Phys. Chem. C* **2008,** *112*, 9872-9879.

10. Rossmeisl, J.; Logadottir, A.; Nørskov, J. K., Electrolysis of water on (oxidized) metal surfaces. *Chem. Phys.* **2005,** *319* (1-3), 178-184.

11. Bianco, E.; Butler, S.; Jiang, S.; Restrepo, O. D.; Windl, W.; Goldberger, J. E., Stability and exfoliation of germanane: A germanium graphane analogue. *ACS Nano* **2013,** *7* (5), 4414–4421.

12. Zhu, Y.-A.; Chen, D.; Zhou, X.-G.; Yuan, W.-K., DFT studies of dry reforming of methane on Ni catalyst. *Catal. Today* **2009,** *148* (3-4), 260-267.

13. Muñoz-García, A. B.; Tuccillo, M.; Pavone, M., Computational design of cobalt-free mixed proton–electron conductors for solid oxide electrochemical cells. *J. Mater. Chem. A* **2017,** *5* (23), 11825-11833.

14. Tsai, C.; Li, H.; Park, S.; Park, J.; Han, H. S.; Norskov, J. K.; Zheng, X.; Abild-Pedersen, F., Electrochemical generation of sulfur vacancies in the basal plane of MoS_2 for hydrogen evolution. *Nat. Commun.* **2017,** *8*, 15113.